Indoor Soiling Method and

Outdoor Statistical Risk Analysis of Photovoltaic Power Plants

by

Vidyashree Rajasekar

A Thesis Presented in Partial Fulfillment
of the Requirements for the Degree
Master of Science in Technology

Approved April 2015 by the
Graduate Supervisory Committee:

Govindasamy Tamizhmani, Chair
Devarajan Srinivasan
Bradley Rogers

ARIZONA STATE UNIVERSITY

May 2015

ABSTRACT

This is a two-part thesis.

Part 1 presents an approach for working towards the development of a standardized artificial soiling method for laminated photovoltaic (PV) cells or mini-modules. Construction of an artificial chamber to maintain controlled environmental conditions and components/chemicals used in artificial soil formulation is briefly explained. Both poly-Si mini-modules and a single cell mono-Si coupons were soiled and characterization tests such as I-V, reflectance and quantum efficiency (QE) were carried out on both soiled, and cleaned coupons. From the results obtained, poly-Si mini-modules proved to be a good measure of soil uniformity, as any non-uniformity present would not result in a smooth curve during I-V measurements. The challenges faced while executing reflectance and QE characterization tests on poly-Si due to smaller size cells was eliminated on the mono-Si coupons with large cells to obtain highly repeatable measurements. This study indicates that the reflectance measurements between 600-700 nm wavelengths can be used as a direct measure of soil density on the modules.

Part 2 determines the most dominant failure modes of field aged PV modules using experimental data obtained in the field and statistical analysis, FMECA (Failure Mode, Effect, and Criticality Analysis). The failure and degradation modes of about 744 poly-Si glass/polymer frameless modules fielded for 18 years under the cold-dry climate of New York was evaluated. Defect chart, degradation rates (both string and module levels) and safety map were generated using the field measured data. A statistical reliability tool,

FMECA that uses Risk Priority Number (RPN) is used to determine the dominant failure or degradation modes in the strings and modules by means of ranking and prioritizing the modes. This study on PV power plants considers all the failure and degradation modes from both safety and performance perspectives.

The indoor and outdoor soiling studies were jointly performed by two Masters Students, Sravanthi Boppana and Vidyashree Rajasekar. This thesis presents the indoor soiling study, whereas the other thesis presents the outdoor soiling study. Similarly, the statistical risk analyses of two power plants (model-J and model-JVA) were jointly performed by these two Masters students. Both power plants are located at the same cold-dry climate, but one power plant carries framed modules and the other carries frameless modules. This thesis presents the results obtained on the frameless modules.

DEDICATION

This thesis work at ASU-PRL is dedicated to my parents, Rajasekar Arunachalam and Padma Rajasekar, and my brother, Karthikeyan Rajasekar, for their constant motivation, love and support during my Master's program.

TABLE OF CONTENTS

LIST OF TABLES

LIST OF FIGURES

PART 1: INDOOR SOILING METHOD

1.1 INTRODUCTION

1.1.1 Background

Soiling is a major source of energy loss on Photovoltaic (PV) modules, and it becomes difficult when considering the quantification of dust influence. Particle size, shape, composition, moisture content, deposition pattern and accumulation rate vary from location to location due to the geography, climate and urbanization of the region [1]. In the context of PV, soiling loss refers to losses primarily due to dust deposition.

Previous studies show that losses due to accumulated dirt on modules can reach as high as 15% for a period without rain [2]. Apart from these losses, there are increasing number of claims of dust resistant coatings, abrasion resistant coatings (during cleaning), and new dust removal techniques. Currently, there is no standardized way of verifying the validity of such claims. As a first step towards validating such claims, a standardized artificial soiling method using a laminated module construction of glass/EVA/cell/EVA/backsheet is developed in this report. Also, the characterization tests that would give all-round information about the soiling losses are identified.

1.1.2 Statement of the Problem

Natural soiling in PV is time-consuming and location specific. The results obtained in natural soiling cannot be generalized due to varying physical and chemical properties of soils across the globe. Hence, there comes the necessity to develop/to speed up the soil

depositing pattern artificially. Accelerated and artificial means of soil deposition can help reduce the time taken to estimate the losses due to soiling and help authenticate such claims of dust resistant properties and dust removal techniques. Pre-characterized soil from different regions can be deposited using this laboratory oriented approach, and the losses can be quantified.

1.1.3 Objectives

One of the main objective is to determine that reflectance and QE measurements can be used as a direct measure to calculate soil density. By measuring reflectance on the soiled modules, reflectance loss (%) is calculated. From reflectance loss, soil density (g/m^2) is calculated and the corresponding I_{sc} drop is determined.
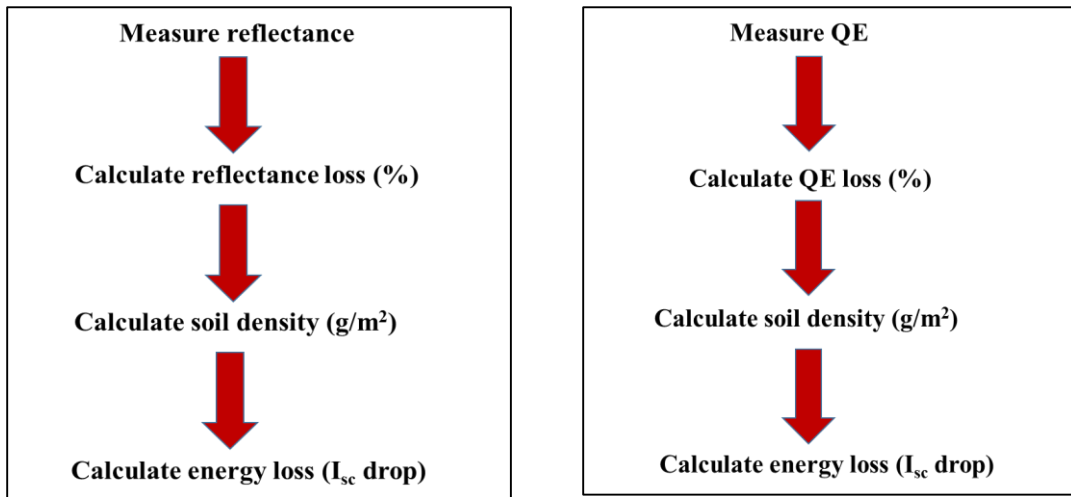
Figure 1. Goal of the experiment

1.2 LITERATURE REVIEW

1.2.1 Artificial Soil Formulation and Application- Sandia's Approach

Burton *et al*. from Sandia National Laboratories have reported a means to deposit and characterize artificial soil coatings composed of NIST- traceable dust with known chemical and physical properties [3]. The process is as follows: Arizona Road Dust (ISO 12103-1, A2 Fine Test Dust nominal 0-80 micron size, Powder Technology, Inc., Burnsville, MN, USA) was mixed with a soot mixture composed of 83.3 % w/w carbon black, (Vulcan XC-723, Cabot Corp, Boston, MA, USA); 8.3 % diesel particulate matter, (NIST Catalog No. 2975); 4.2 % unused 10W30 motor oil, 4.2 % α-pinene, (Catalog No. AC13127-2500, Acros Organics, Geel, Belgium) in a glass jar and tumbled without milling media in a rubber ball mill drum at 150 r/min for 48 to 72 h. The composition was varied to include 3 wt%, 10 wt%, and 25 wt% soot mixture and samples were prepared on a 100 g total solid basis. The composition of the varying soot mixture did not represent any specific location, but on an average, represented the soot content present in a few locations.

For application onto the samples, this grime mixture was combined with Acetonitrile, ACN (HPLC grade, Sigma Aldrich, St. Louis, MO, USA) in a ratio of 3.3 g to 275 ml and was sprayed on a commercial glass coupon (7.62 cm $\times$ 7.62 cm). The grime mixture was sprayed using a HVLP (High velocity Low Pressure) gun held approximately 30 cm from the coupon surface. The samples were sprayed from right to left for a duration of 1‑3 seconds, and to obtain high soiling density, multiple coatings were sprayed. The glass

coupons before and after soiling were weighed with a Mettler Toledo (Columbus, OH, USA) XP205 balance with 0.00001 g resolution and characterization tests were also performed. Variations in the grime mixture was produced by incorporating major optical components, like iron oxide and in-house synthesized göthite, as primary spectral components.

After soil formulation and application, characterization tests like current-voltage and QE measurements, were carried out on soiled glass samples and the results are discussed.

1.2.2 Reflectance Spectroscopy- An Overview

Reflectometery (or reflectance spectroscopy) is used in a variety of metrological applications for determination of chemical composition, material identification, and measurement of optical properties of materials [4]. Reflectance on PV modules can be reduced by the introduction of anti-reflective (AR) coating or texturing of the glass surface.

In the case of cleaned modules, the reflectance (between 350-2500 nm) on a module surface can measure surface roughness, surface cleanliness, contamination, texturing, AR coating properties, and metallization parameters. For soiled modules, as soil is deposited on the surface, reflectance curve can be used to determine the physical composition, chemical composition and properties of the soil. The prediction of various components between 350-2500 nm is given in the table as follows:

Table 1. Prediction of Various Components in Reflectance Spectra [5]

Wavelength (nm)	Predicted components
350-400	Eliminated due to noise
400-1100	Iron oxide content
600	Anti-Reflection coating
600-900	Soil Organic Content (SOC)
1900-2200	Clay content
1900-2300	Carbonate content
1400, 1900 and 2200	Water absorption peaks

1.3 METHODOLOGY

1.3.1 AZ (Arizona) Road Dust

Soils were formulated artificially by mixing standardized soil or particulate matter, commonly referred to as AZ road dust (ISO 12103-1, A2 Fine Test Dust) with HPLC (High Performance Liquid Chromatography) grade acetonitrile.

According to the manufacturer, the raw material for Ar road dust is the dust that settles out of the air behind or around tractors operating in the Salt River Valley, Arizona. They are recommended to be caught on a canvas cloth and are dried in an oven. The dried dust is made to pass through 200 mesh screen (0.0029 in. width of openings) and the dust that stays on the mesh is discarded. The dust that is obtained is finally made to pass through 270 mesh screen (0.0021 in. width opening) and is collected. The chemical composition and the test dust particle size is included in APPENDIX-A.

1.3.2 Spray Gun Specifications and Adjustments

The solution is then uniformly sprayed on the test module using a HVLP (High Velocity Low Pressure) spray gun with a 1 mm nozzle from Centralpneumatic. The detailed specifications of the spray gun are as follows:

Table 2. Spray Gun Specifications [6]

Item	Gun used
Air Pressure Range	30 - 40 PSI
Maximum Air Pressure	40 PSI
Air Consumption	12 CMF @ 40 PSI
Cup Capacity	20 fl.oz.
Air Inlet	¼" - 18 NPS

Three factors that need to be considered during spray gun adjustment stage are:

1. Fan direction

2. Pattern adjustment

3. Fluid adjustment

After soiling, the variation in density was found to be high along a particular direction. If the fan of the gun was placed along a horizontal direction, it was observed that the variation in density was high in the slides that were placed along a vertical direction, and vice-versa when the fan was adjusted along a vertical direction. For this study, the fan of the gun was constantly fixed along a horizontal direction, and the microscopic slides to calculate soil density were placed along a vertical direction so the variation was controlled.
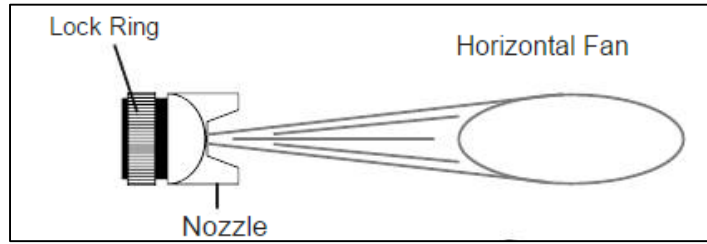
Figure 2. Horizontal Fan Direction [6]

Based on trial measurements, it is identified that when the pattern knob was adjusted to round/closed position the soil spray was more uniform. The pattern knob was used to adjust the spray pattern.
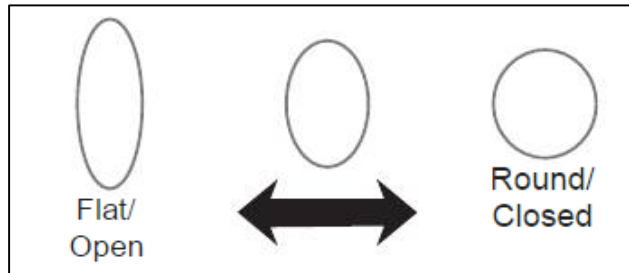
Figure 3. Pattern Adjustment [6]

The fluid knob was adjusted to a fine position and the air pressure was set to 30 PSI to get a fine layer of soil on the test modules.
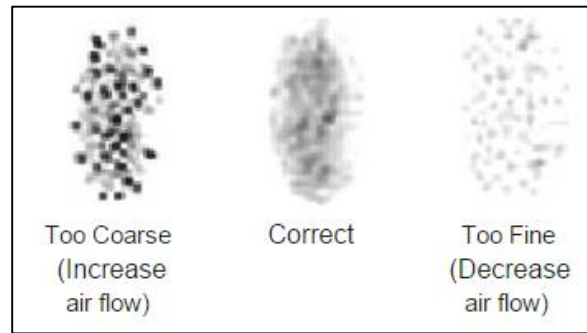
Figure 4. Fluid Adjustment [6]

1.3.3 Soil Formulation

Initially the suspensions were prepared to have a composition of AZ road dust mixed with acetronitrile (ACN) in a ratio of 3.3 g to 275 ml. While spraying soil, it was found that formulated soil from the gun did not reach the test module and resulted in a thin layer of soiling even after many rounds of application. Hence the composition was changed to 15 g of AZ road dust for every 1000 ml of acetonitrile. By varying the composition of ACN, different soil densities were obtained, and a density of above 1.8 g/m^2 led to clogging in the spray gun.

1.3.4 Test Coupons

Polycrystalline and monocrystalline silicon coupons with no AR coating were used in this study. Polycrystalline silicon mini-modules of construction Glass/EVA/Cell/EVA/Backsheet having an aperture area of 144 cm^2 was used. Each mini-module was comprised of 18 polycrystalline silicon cells that are series connected. The dimensions of each cell are 5.7 cm $\times$ 1 cm and are rated to produce 1.48 W.

10

A single-cell monocrystalline silicon coupon also had the same construction as Poly Si. The area of the cell was found to be 225 cm^2 (15 cm×15 cm). As an attempt to characterize the optical properties of soil using spectroradiometer, this coupon was laminated such that there was extra space close to the cell.

Table 3. Specifications for Poly and Mono-Si Coupons

Variables	Poly-Si (Multi-cell coupon)	Mono-Si (Single-cell coupon)
Coupon structure	Glass/EVA/Cell/EVA/Backsheet	Glass/EVA/Cell/EVA/Backsheet
Number of cells	12 cells in series	1 cell
Cell dimension	5.7 cm by 1cm	15.4 cm by 15.4 cm
Total cell area	144 cm^2	233 cm^2
I_{sc}	0.18 A	9.33 A
V_{oc}	10.71 V	0.59 V
P_{max}	1.48 W	3.5 W
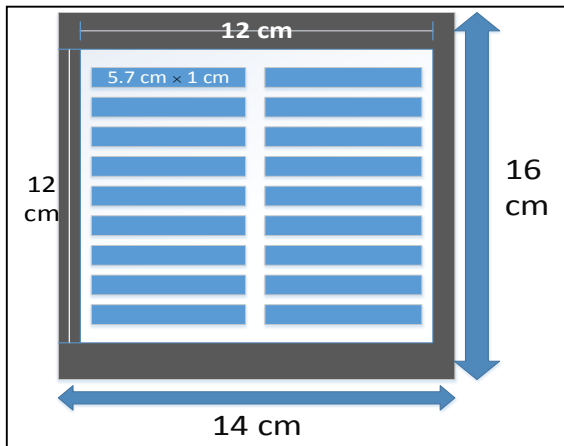
Figure 5. (a) Polycrystalline Silicon
Mini-module
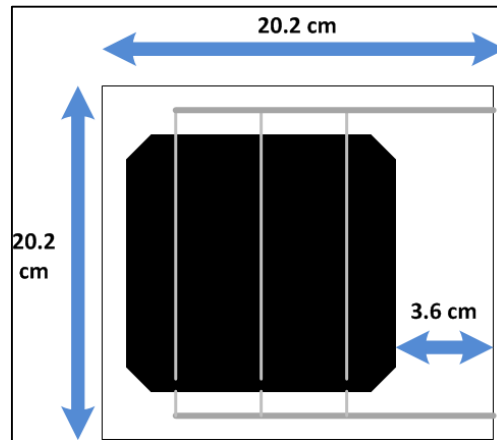
(b) Single-cell Monocrystalline Silicon

1.3.5 Artificial Chamber Set Up

To maintain a controlled environment during soil deposition, an artificial chamber was constructed. The chamber consisted of a cuboidal mechanical structure to support an air bag from Sigma Aldrich Corporation. In order to avoid human errors, the spray gun was placed on a mechanical structure and the soil was sprayed. The distance between the test coupon and the tip of the gun was ensured to be about 2.5 feet.

The artificial chamber was initially erected horizontally, but on spraying soil, it was observed that the soiling pattern was more uniform when the chamber was flipped (placed vertically) and the coupon was placed on the ground, as gravity helps in maintaining uniformity. Also, it is important to ensure that the spray gun was held perpendicular to the center of the module and a pulse-spray approach was implemented to obtain further uniformity.

12

Figure 6. Artificial Chamber (60*46*76, in cm) Erected Horizontally (Without Glove Bag)

Figure 7. Erected Vertically (With Glove Bag)

1.3.6 Importance of Laser-Guided Technique

Initially, the laser pointer was not employed during the application of soil, and on weighing the microscopic slides, the maximum deviation in density between two slides was found to be 0.6 g/m^2. To further increase the accuracy, a laser pointer was attached to the tip of the gun as shown in Figure 6(b). The laser spot helped in determining the exact center of the test coupon while spraying, and maximum deviation in density was reduced to 0.2 g/m^2.

Figure 8. Spray Gun (a) Without Laser Pointer   (b) With Laser Pointer

1.3.7   Soil Density Measurements

The soil density measurements (g/m^2) were carried out using commercially available microscope slides (2.5×7.6 cm) placed on two sides of the test coupon. The density calculations were carried out using Mettler Toledo (AG285, resolution 0.001 mg). The soil density was calculated by measuring the difference in the weight of the slides before and after soil deposition, divided by the area of the microscopic slide. The average of these measurements was taken to determine soil density on the mini-module.
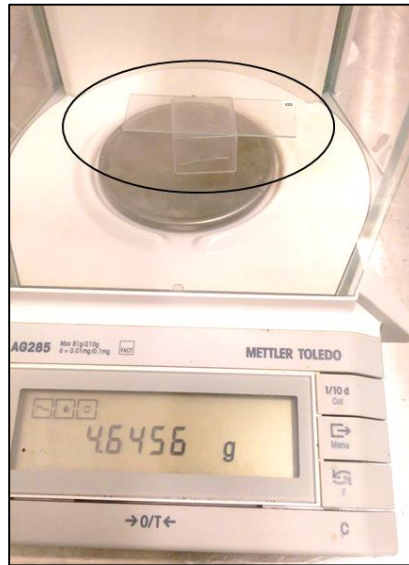
Figure 9. Soil Density Calculation (Soiled Microscopic Slide Circled)

1.3.8 Poly-Si Coupon‑ Good Indicator of Uniformity

To verify the uniformity in soiling pattern using this approach, I-V curves were taken before and after soiling on the polycrystalline Si coupon (as multiple cells are connected in series). If there exists any significant non-uniformity, then no smooth curve would be expected between I_{sc} and I_{mp} values.

The soiled poly-Si coupons went through a few characterization tests as indicated in the flow diagram (Figure 15). Uncertainties that were observed during the characterization tests like reflectance and quantum efficiency on poly-Si was noted. In order to overcome these above stated uncertainties and to get accurate measurement results, the same process was followed on monocrystalline silicon coupons.

1.3.9 Spectroradiometer – Instrument Overview

A FieldSpec-4 UV-Vis-NIR reflectance spectroradiometer from Analytical Spectral Devices (ASD), Colorado was used for all the reflectance measurements. In addition to reflectance, the instrument can measure transmittance and irradiance as it is a special kind of spectrometer that can measure radiant energy. It is a compact, field portable and precision instrument which has a spectral range of 350–2500 nm and a fast data collection time of 0.2 seconds per spectrum. The instrument has a fixed optic cable that helps to calibrate to units of radiant energy (irradiance and radiance), and it is operated using a computer that has RS^3 software installed. This instrument is extensively used by the agricultural industry for analyzing soil samples.

Figure 10. High Resolution Spectroradiometer [7]

Figure 11. Contact Probe [7]

Table 4. Technical Specifications of Spectroradiometer [7]

Spectral Range	350-2500 nm
Spectral Resolution	3 nm @ 700 nm
	8 nm @ 1400/2100 nm
Sampling Interval	1.4 nm @ 350-1050 nm
	2 nm @ 1000-2500 nm
Scanning Time	100 milliseconds
Stray light specification	VNIR 0.02%, SWIR 1 & 2 0.01%
Wavelength reproducibility	0.1 nm
Wavelength accuracy	0.5 nm

The front panel consists of an accessory power port and a fiber optic cable that is fixed. The cable should be handled with care as it tends to break on bending; any breakage in the cable can be identified using the fiber optic checker, and can be replaced if the Signal to Noise Ratio (SNR) drops below an acceptable level. The instrument back panel has an on/off switch that allows the instrument to switch on/off accordingly, and an Ethernet port that is to be connected to the laptop that has the software installed in it. The power port supplies power that is required by the instrument and is connected to the instrument controller. A Nickel‑Metal Hydride (NiMH) battery is also provided to assist in outdoor measurements [8].

Setting up and saving spectrum

- For reflectance measurements, the light source should be switched on for a minimum of 15 minutes. The contact probe acts as a light source and also as a receiver.

- Before taking any reading, the instrument needs to be optimized to the current atmospheric conditions or else the instrument gets saturated.

- The calibrated white reference (WR) reflector is fixed to the contact probe and the reflectance is collected. A straight line at 1 is observed, indicating that all light is reflected (as it is white), and with respect to this, all other reflectance measurements are carried out.

- The white reference cap is removed, the contact probe is perpendicularly placed on the coupon surface and spectrum is saved to collect reflectance.

- The reflectance values are saved as .asd files and they are converted to .txt files using ViewSpecPro software.

The detailed procedure for collecting and saving spectrum is provided in APPENDIX-B.

1.3.10 Quantum Efficiency Measurement System

Quantum efficiency (QE) is defined as the ratio of the number of electron carriers generated to the number of photons of a given wavelength that are incident on the solar cell. QEX12M quantum efficiency measurement system (as shown in Figure 10) is a device that measures QE of a cell within a module using a non-intrusive approach [9].

Figure 12. QEX12M Module QE System [10]

System calibration and operation

To turn the machine on, first turn the main power switch on and then proceed to turn on the auxiliary power switches. After starting up, give the xenon arc lamp about 10-15 minutes to warm up. The module bias light should be turned on. The intensity of the light can be adjusted by turning the knob.

Always start by calibrating the system before taking QE measurements. Position the monochromatic light on the calibration photodiode. Select 'Calibration PD' on the home screen. Measure the calibration curve by clicking start. After the curve is finished, save the curve and select 'apply as calibration'. The monochromatic beam is then positioned on the test coupon and by applying voltage bias and light bias, the QE measurements are carried out.

1.3.11 Characterization Techniques

The test coupon was first cleaned with tap water, followed by distilled water and finally with isopropyl alcohol. EL imaging was done on a cleaned module to look for any localized defects as QE measurements are to be done on the module.
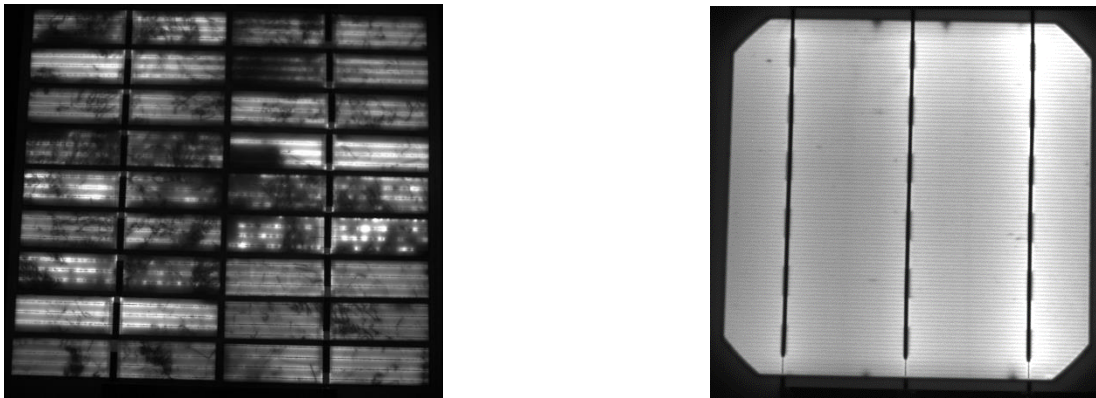
Figure 13. EL Image (a) Poly-Si   (b) Mono-Si

IV characterization was done on a cleaned module to observe whether or not the curve is smooth, as it gives an idea about the health of the test module. Followed by I-V, soil is sprayed on the module uniformly, and various density soil is obtained by varying the concentration of acetonitrile solution. The soiled module undergoes soiled I-V characterization to understand the I_{sc} loss for different soiling densities. According to EL image, two spots on the test module were chosen and soiled reflectance was carried out.

Figure 14. Reflectance
Measurements on (a) Poly-Si

(b) Mono-Si

After soiled reflectance, a soiled QE measurement was performed using QEX12M Solar Module Quantum Efficiency Measurement System (PV Measurements). Since the polycrystalline module had 18 cells, it was important to keep the cell of interest completely in the dark. Hence, a mask was cut exactly to the size of the cell and a small window was provided so the light source can reach the module (as shown in Figure 14). Another existing feature is the shroud, but as the usage of this might disturb the soiling layer, it was not used. Individual voltage bias was applied and by keeping the voltage bias constant, multiple QE was taken (due to grain boundary effect) for each spot, and the average was considered to be the QE of that spot. The light bias was always maintained at 100% intensity.

Monocrystalline silicon, being a single cell module, had no necessity in using voltage bias. The light bias was maintained at 100% intensity similar to poly-Si. Identical QE curves were obtained along any place in the spot and proved to be more accurate.
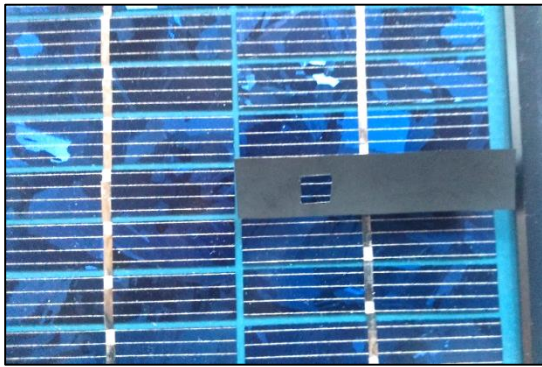
Figure 15. (a) Poly-Si Cell Covered with   (b) Mono-Si cell with Light Source

Mask (An Opening for Light Source)
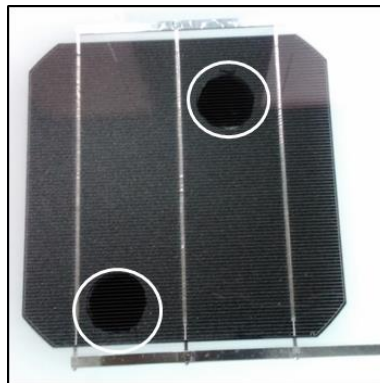
Figure 16. Soiled Spots Cleaned for Reflectance and QE

Also, it was made sure that QE was performed on the same spot where reflectance was done. The soil layer that was present in the spots were cleaned using cotton gauze dampened with isopropyl alcohol. Finally cleaned QE and reflectance measurements were performed.
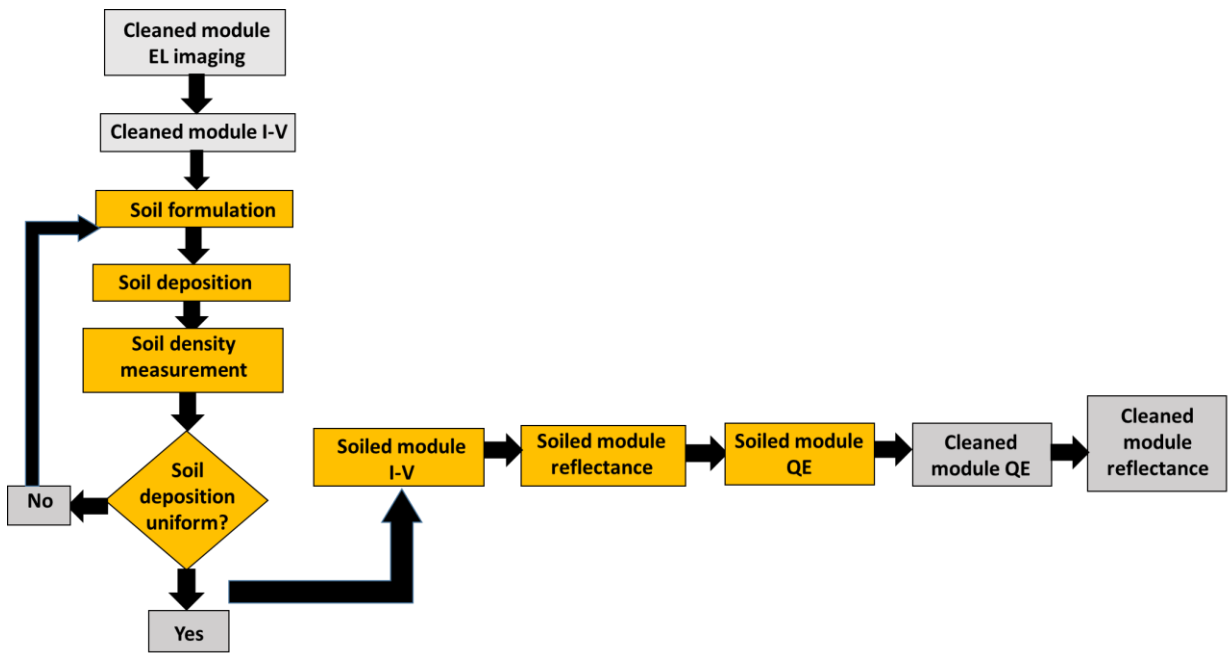
Figure 17. Flow Chart Indicating the Characterization Process

1.4 RESULTS AND DISCUSSIONS

1.4.1 Soil Uniformity Check

To check if the soil layer obtained using this approach is uniform, four microscopic slides were placed on four sides of the coupon. A laser-guided technique was used during soil application and the slides were weighed before and after cleaning. The standard deviation for all four soil densities was found to be 0.02%, which is a very good indication that the process is uniform.
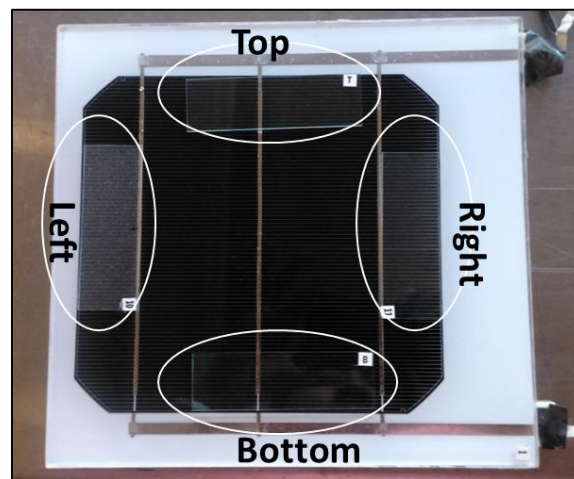
Figure 18. Coupon Containing Microscopic Slides
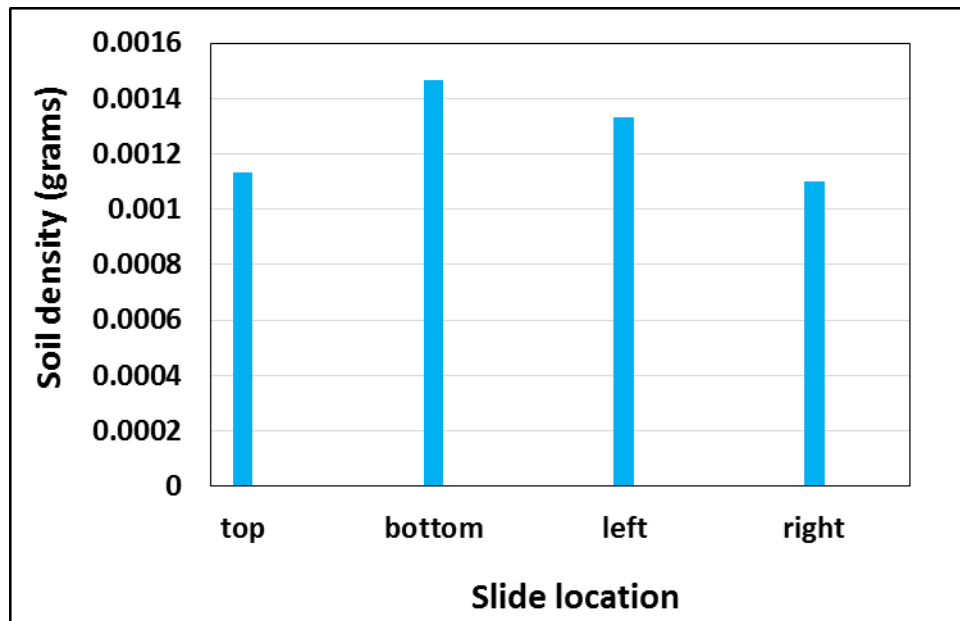
Figure 19. Slide Location Vs Soil Density

1.4.2 Process – Sample Size Independent Repeatability

Poly-Si modules were coated with different soil densities ranging from 0.6 to 1.55 g/m^2 [11], and single cell modules were also coated with densities ranging from 0.18 to 1.8 g/m^2 as shown in Tables 5 & 6. In Table 6, soiling densities 1.57 g/m^2 and 1.8 g/m^2 almost had the same I_{sc} loss, meaning the process is repeatable. The uniformity pattern was observed in both Poly-Si and mono-Si modules of sample size 144 cm^2 and 225 cm^2 respectively. This indicates that the soil spraying process holds good for various size coupons.

Table 5. I_{sc} Loss for 144 cm^2 (Poly-Si)

Mini Module	Soil Density (g/m^2)	I_{sc} loss
1	0.60	2%
2	0.80	2.25%
3	1.08	5.48%
4	1.55	8.24%

Table 6. I_{sc} Loss for 233 cm^2 (Mono-Si)

Soil Density (g/m^2)	I_{sc} loss
0.180	1.4%
0.34	1.3%
0.62	2.4%
0.92	3.8%
1.57	8.1%
1.8	8.2%

Figure 18 shows a linear dependence in I_{sc} loss with respect to soil density. The I_{sc} loss is the difference between cleaned I_{sc} and soiled I_{sc} divided by cleaned I_{sc}. This plot indicates that the I_{sc} values can be used to measure the soil density or soil loss for the experimental variables used in this work.
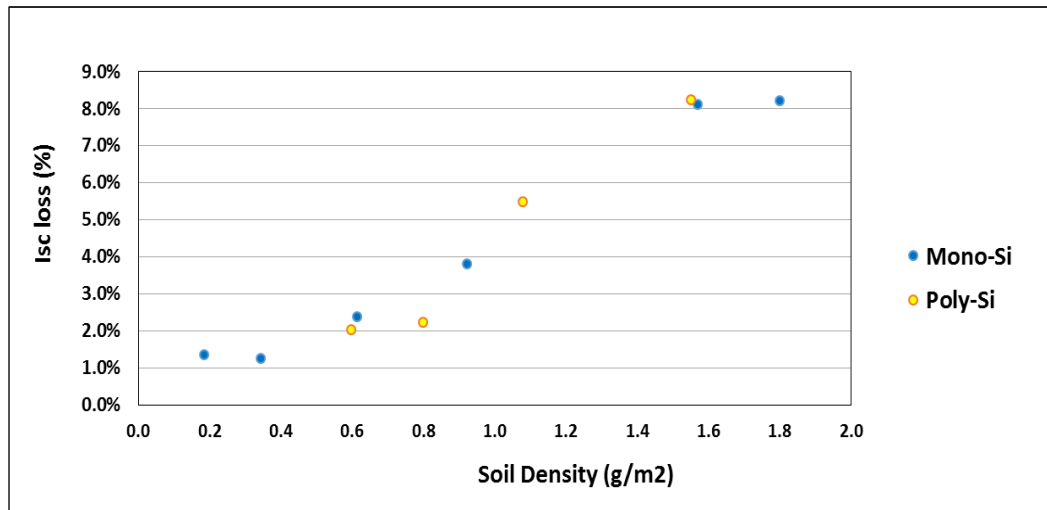
Figure 20. Soil Density (g/m^2) vs I_{sc} Loss (%)

26

1.4.3 Mono-Si‑Better Technology to Characterize QE and Reflectance Losses

For reflectance measurements, the contact probe diameter of spectroradiometer was found to be larger than the cell area of the polycrystalline mini-module. Instead of covering one cell at a time, the contact probe covers two cells that are shown using the circle in Figure 19. Hence, this resulted in noise in the reflectance measurements.
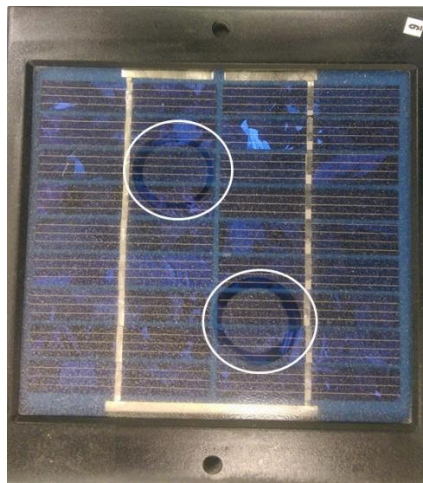
Figure 21. Circle Indicating Contact Probe Diameter>Cell Area for Poly-Si Coupon

When comparing the Quantum Efficiency (QE) measurements for both poly and mono-Si, the influence of grain boundaries on poly-Si infused noise in the results. On the other hand, mono-Si, being a single cell module, eliminated these noises. Figures 20 & 21 show the variation in QE curve for both poly and mono-Si modules. The variation in QE curve for mono-Si (both cleaned and soiled) is minimal and it clearly proves that in order to eliminate noises and to obtain accurate results in QE measurements, mono-Si samples should be preferred.
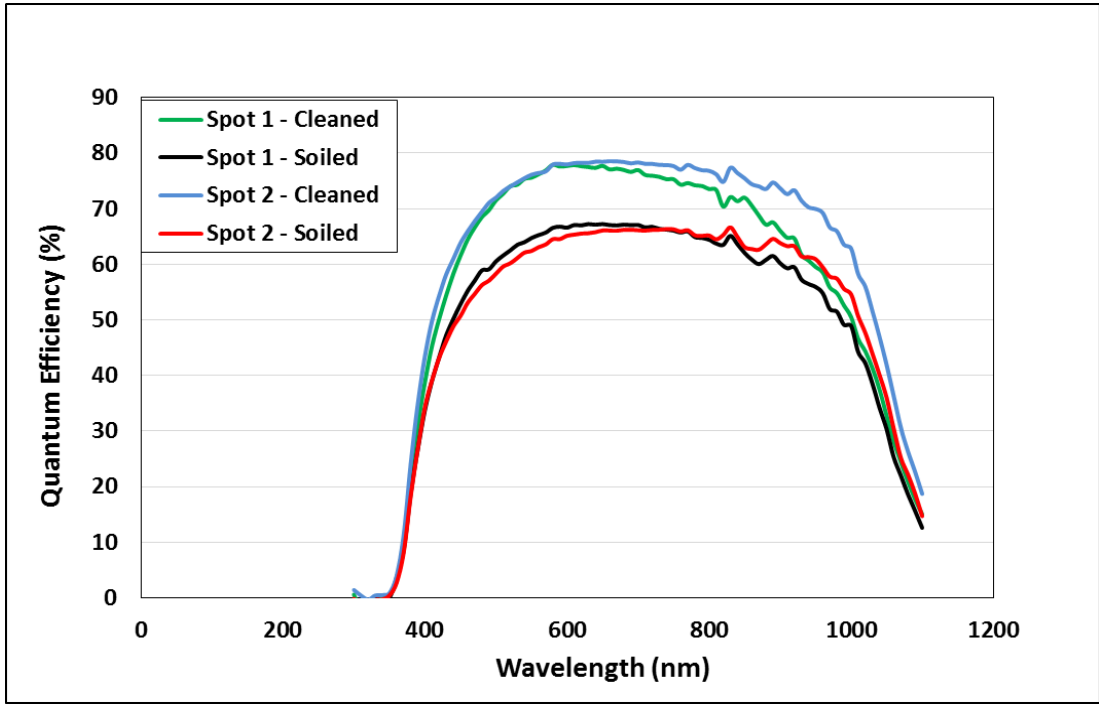
Figure 22. QE Curve for Poly-Si Coupon (1.55 g/m^2)
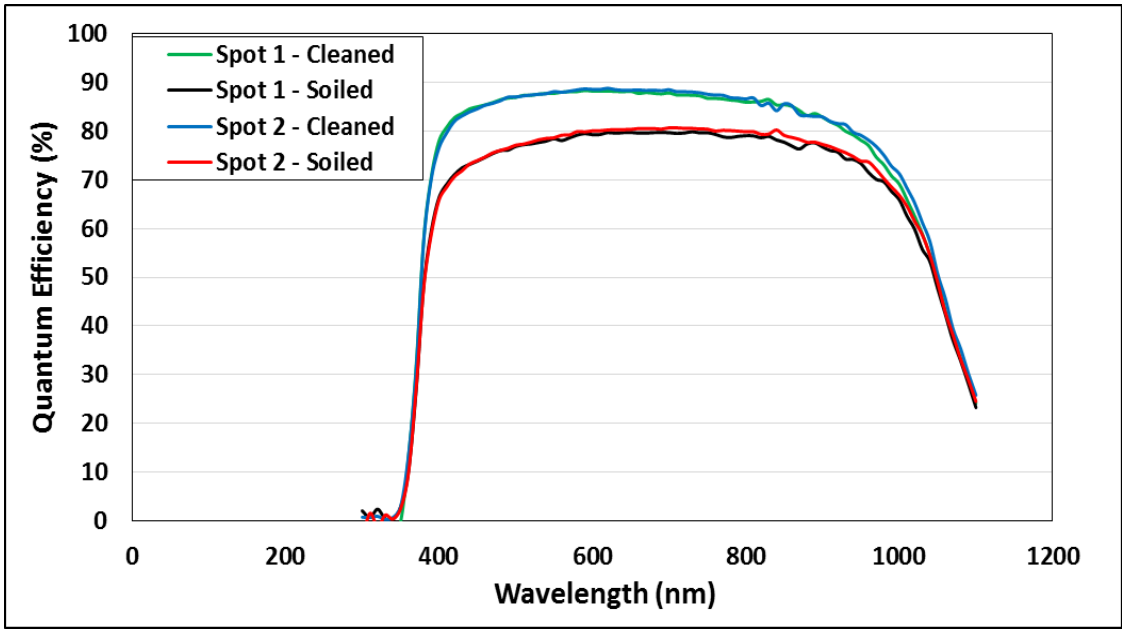
Figure 23. QE Curve for Mono-Si Coupon (1.57 g/m^2)

28

1.4.4 Relation between Cleaned QE and Reflectance

Considering Figure 22, the drop in wavelength below 1100 nm is due to the cell absorption, as the absorption region of c-Si is below 1100 nm. From 1000 nm, the reflectance increases as the QE curve starts decreasing. The dip at 1700 nm is due to EVA (Ethylene Vinyl acetate) absorption. If the property of EVA changes over time, then the dip varies accordingly.
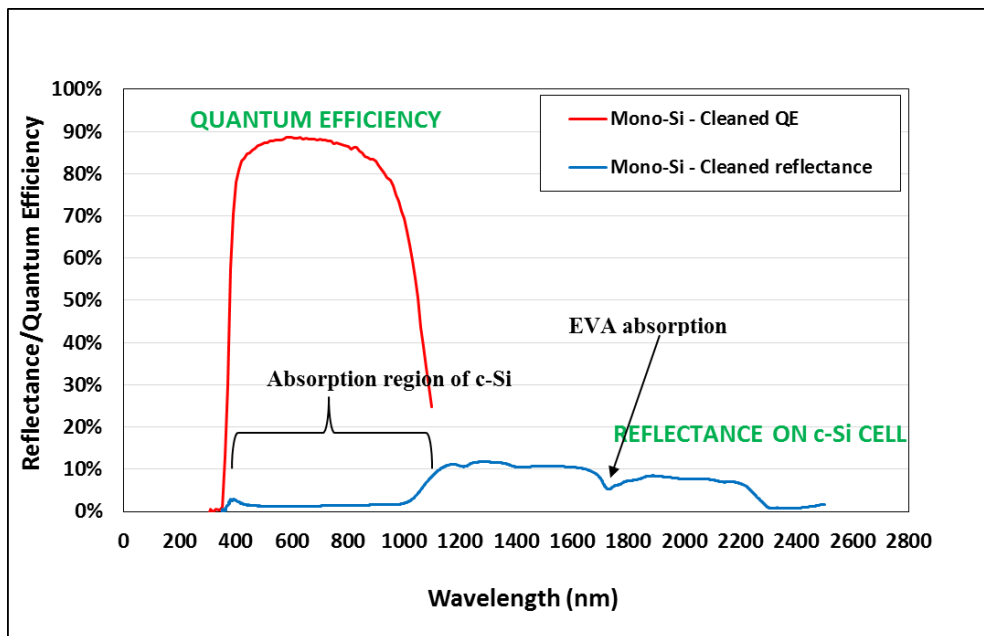
Figure 24. Graph between Cleaned QE and Reflectance for Mono-Si

1.4.5 Glass/EVA/Backsheet Reflectance

The white area refers to the area that is sandwiched between Glass/EVA/White backsheet. The backsheet reflectance decreases as the wavelength increases, and most of the peaks

that are seen are mainly due to the backsheet properties. Also, any changes in the encapsulant layer/backsheet can be determined from Figure 24.

Figure 25. Contact Probe on White Area for Reflectance Measurements (see Figure 16 for the full size picture of the 1-cell coupon)
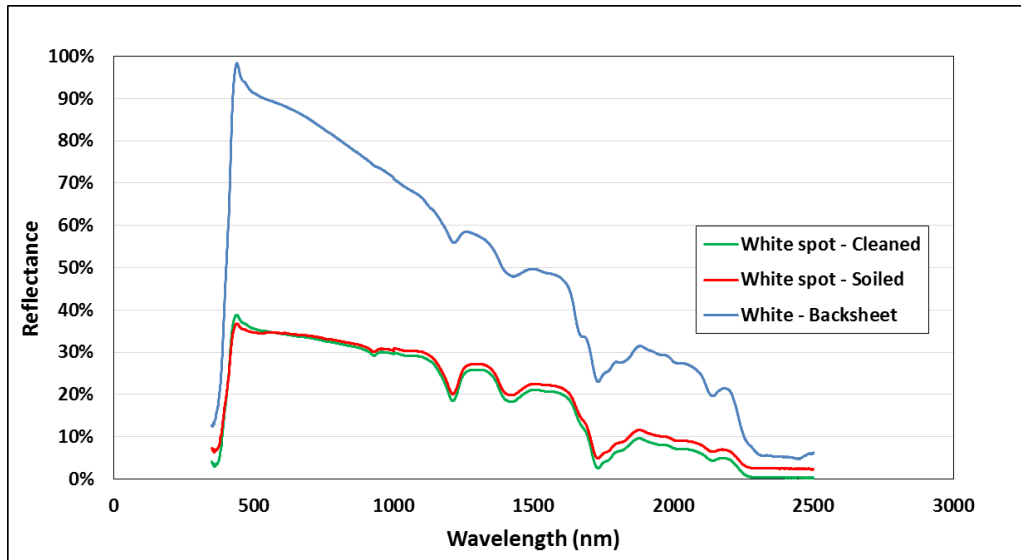
Figure 26. Reflectance Plot for White Area and White Backsheet

1.4.6 Reflectance (Soiled %-Cleaned %) Plots for Various Soil Densities

The reflectance plots for various soil densities ranging from 0.18 g/m^2 to 1.8 g/m^2 is shown in Figure 25. From the graph below, it is evident that the reflectance increases as the soiling density increases. For all soil densities, maximum reflectance was found to be between 400-1100 nm, which corresponds to the absorption region of c-Si.
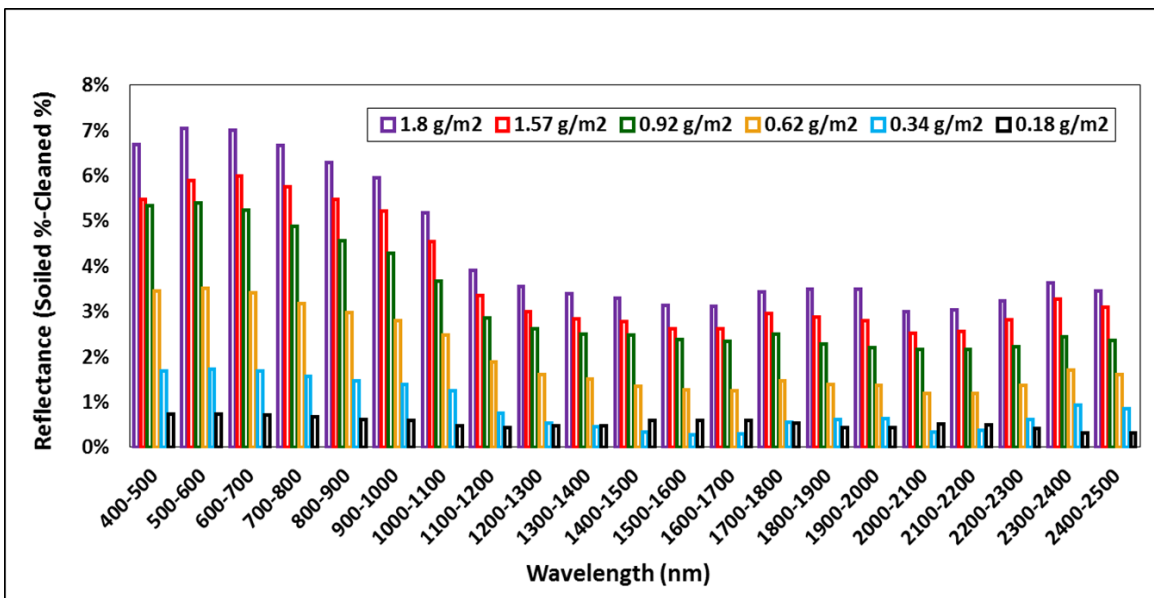
Figure 27. Reflectance (Soiled %-Cleaned %) Plots for Various Soil Densities

1.4.7 Particle Size Effect on Reflectance

When comparing the outdoor and indoor reflectance, the outdoor reflectance curve over the absorption region seems to be uniform (flat), whereas for indoor, it was observed to be non-uniform. Bowers *et al.* showed that reflectance increased with a decrease in particle size and this effect was more prominent for a particle size less than 400 microns, which is

possibly true in the case of indoor soiling [12]. As scattering increases, the wavelength decreases. The scattering effect due to fine particle size, could be the reason for non-uniformity patterns observed in indoor reflectance measurements.
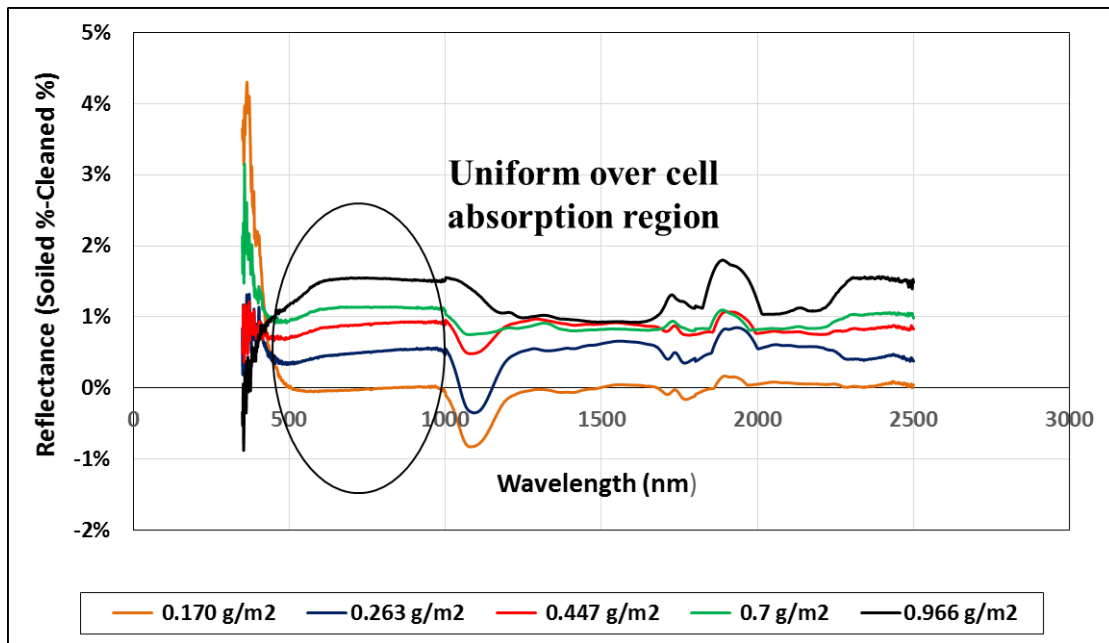
Figure 28. Outdoor – Reflectance Plots for Various Soil Density
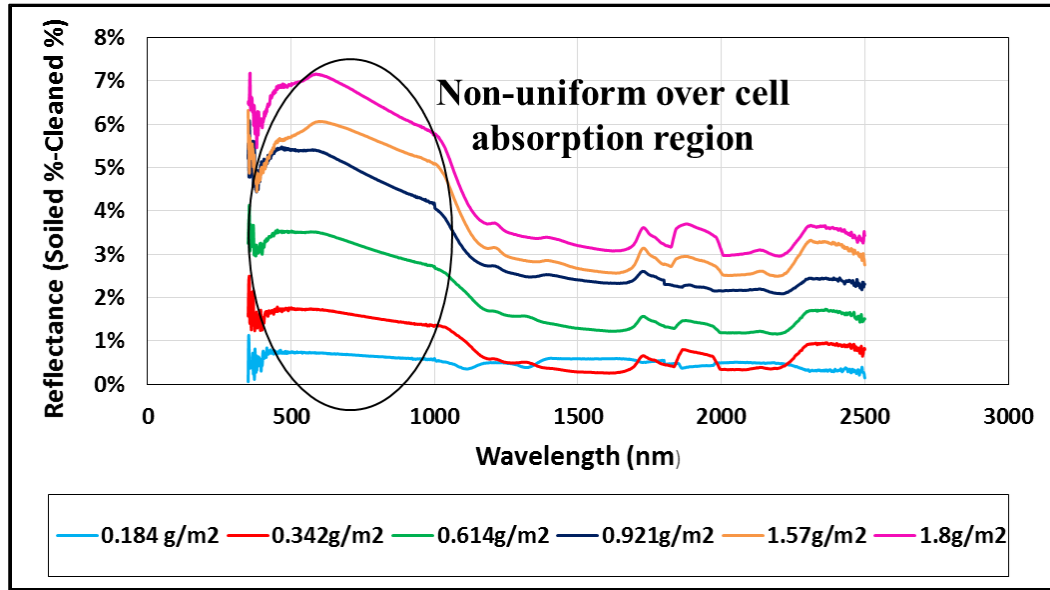
Figure 29. Indoor – Reflectance Plots for Various Soil Density

1.4.8 Reflectance Measurements – A Measure of Soiling Density

Delta (soiled %-cleaned %) for reflectance measurements is calculated for each soil density. The slope of the data is calculated and the R^2 value is determined for all the wavelengths ranging from 400 to 2500 nm. The wavelength between 600-700 nm showed an acceptable R^2 value of 0.918. Similarly, for outdoor soiling, the wavelength between 600-700 nm was determined to be a good fit, irrespective of the technology for measuring density. The equation is as follows:

$$\text{Soil density} \left(\frac{g}{m^2}\right) = 25.35 * \text{average reflectance loss}(\%) - 0.36$$

33

The correlation plot between QE and soil density (Figure 29), reflectance and soil density (Figure 30), and transmittance (I_{sc} loss) and soil density (Figure 18) is linear. This further indicates that both reflectance/QE can be confidently used to determine soil density without collecting soil from the module surface, and the energy loss (I_{sc} loss) can be calculated using the reflectance loss.

Recommendations

- Instead of single cell coupons, modules can be soiled artificially by increasing the distance between the chamber and spray gun.

- Artificial soil formulation ad application, as mentioned above, can be extended for various soils across the globe and characteristics can be determined.

- Similar to outdoor AOI (Angle of Incidence), indoor AOI measurements can be performed for artificially soiled coupons and results can be compared.

- Results obtained by measuring reflectance on PID cells can give a brief description about AR coating.

1.5 CONCLUSION

The study presented largely follows the procedure developed by Burton *et al*. and major conclusions resulting from this study are as follows:

- Gravity-assisted and laser-guided approach of spraying soil onto coupons helps in improving the soil uniformity pattern, and total area of the test coupon for soil application can be further increased by increasing the distance between the module and spray gun.

- Mini-modules can be used to check uniformity by measuring I-V curves, wherein, for characterization tests, single-cell coupons are more favorable.

- Properties of encapsulant (EVA) over time can be determined by carrying out reflectance measurements.

- Particle size plays an important role in reflectance measurements. The smaller the particle size, the higher the reflectance. Also, scattering effect is dominant for smaller particles.

- Reflectance/QE loss can be used as a direct measure of soil density. The correlation plot between soil density (g/m^2), reflectance loss (%) and QE loss (%) varying linearly is shown in Figures 29 & 30.
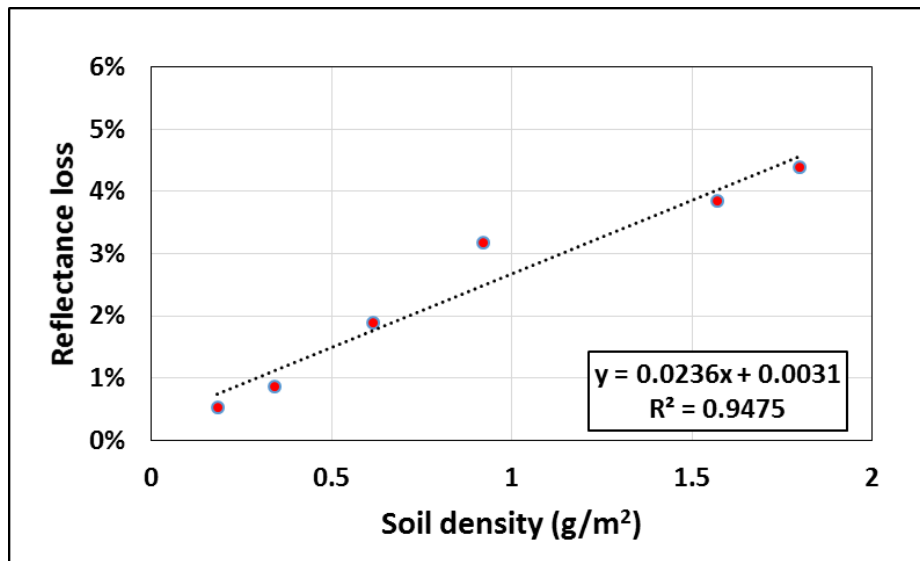
Figure 30. Correlation plot between reflectance and soil density (g/m^2)
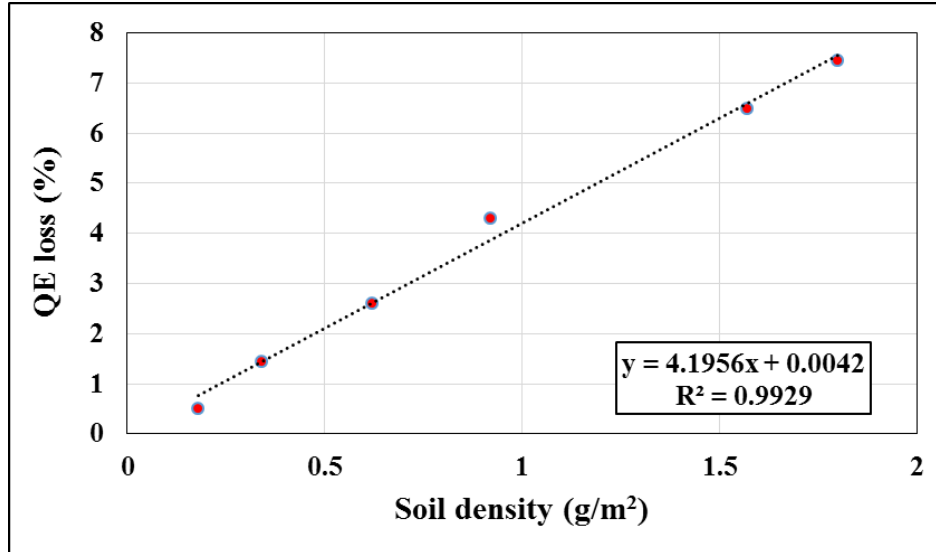
Figure 31. Correlation plot between QE and soil density (g/m^2)

The indoor and outdoor soiling studies were jointly performed by two Masters Students, Sravanthi Boppana and Vidyashree Rajasekar. This thesis has presented the results obtained from the indoor soiling study, whereas, the other thesis presents the outdoor soiling study.

Key findings of the outdoor soiling study are presented below:

- If there is an identical soil density on PV modules, then the relative optical response at different AOI, i.e. f_2(AOI), will be nearly identical, irrespective of the PV technology type.

- The power or current loss between clean and soiled modules would be much higher at a higher AOI than at a lower AOI leading to excessive energy production loss of soiled modules on cloudy days, early morning hours and late afternoon hours.

- Based on the results obtained in this study, it can be stated that the critical angle shifts from 57° for the clean air/glass interface to 40° for the naturally developed air/soil/glass interface in Mesa, Arizona for fall season (0.648 g/m^2 soil density).

- Using an average reflectance measurement between 600-700 nm bandwidth, the soil density of the module can be determined. By using the empirical formula presented in this work, f_2(AOI) values for any AOI, as well as transmission losses, can be estimated if the soil density is known/measured.

- If the soil density of a particular region is known, the angle of incidence related losses for the whole year can be modelled using PVSyst.

PART 2: OUTDOOR STATISTICAL RISK ANALYSIS OF PHOTOVOLTAIC

POWER PLANTS

2.1 INTRODUCTION

2.1.1   Background

Photovoltaic (PV) modules employed in the field can experience different types of failure mechanisms and varying degradation rates due to the changes in environmental conditions, design, installation type, electrical configuration and many other factors. The industry is in need of coming up with appropriate accelerated tests for new modules and in order to achieve this, statistical analysis of performance parameters is necessary to determine degradation modes responsible for the degradation of those parameters. Also, in order to find the dominant failure modes in the modules employed, there is a need to carry out quantitative analyses like FMECA (Failure Mode Effect Criticality Analysis).

FMECA is carried out by ranking and prioritizing the failure modes. It uses the RPN (Risk Priority Number) technique, which is a multiplication of Severity, Occurrence and Detection for ranking the failure modes. The higher the RPN, the worse is the failure mode.

Arizona State University-Photovoltaic Reliability Laboratory (ASU-PRL) has recently evaluated crystalline silicon PV power plants in the State of New York, a cold-dry climatic condition. This site has 18-year-old frameless glass/polymer modules on a rooftop (41° tilt). Sanjay *et al.* [13] was successful in determining the global RPN and in identifying the dominant failure and degradation modes for the hot-dry desert climate of Phoenix, Arizona. In this study, apart from the global RPN, degradation RPN and safety RPN for both string and module-levels have been determined. Safety RPN gives information on the order of

priority for the defects to be addressed which would cause property damage or personnel electric shock. Degradation RPN provides information on the order of priority for the defects to be addressed which would affect the energy production.

2.1.2 Statement of the Problem

There are various field failure modes affecting the safety, reliability and performance of the PV modules. These failures are not unique and as they vary according to the climatic conditions, there needs to be a statistical tool to determine the dominant failure modes. FMECA is one such tool and by determining the failure modes, the module designs that are resistant to those failure modes specific to that climatic condition can be manufactured.

2.1.3 Objectives

The main goal of RPN is to determine the health of the power plant by prioritizing the failure modes and allocating rank accordingly. The eventual goal of RPN study would be to classify power plants into classes based on their Safety RPN and Degradation RPN as shown in Figure 31. The class boundaries would be climate specific.
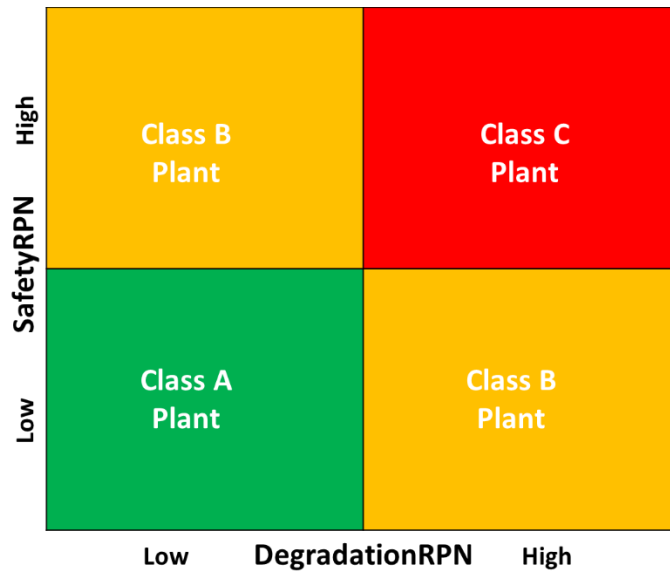
Figure 32. Grading PV Power Plant- Conceptual Approach

The other objectives of this study are:

i.   To determine the String and module-level degradation of power (%/year) by using the field measured data;

ii.   To generate a safety map for the entire power plant that includes all the modules that had safety issues;

iii.   To determine the safety and reliability failures involved;

iv.   To determine the RPN for the failure modes present (both string and module-level) and to rank them accordingly.

2.2 LITERATURE REVIEW

2.2.1   Field Failure and Degradation Modes

Field failure, degradation mode and mechanisms of PV modules depend on the design/packaging/construction in which the modules operate [14]. These failures can further be classified as reliability and durability losses. A few of the field failures are: broken interconnect, broken cells, corrosion, delamination, bypass diode failure, and hot spots. The above stated failure modes are caused due to the failure mechanisms.

Failure mechanism (cause) $\longrightarrow$ Failure mode (effect)

The failure mode/defects can be identified by performing a visual inspection on modules or by using tools to determine the failure.

2.2.2   Reliability Failures

A reliable PV module may also be defined as a PV module that has a high probability of performing its intended function adequately for 30 years under the operating conditions encountered [14].

All modules degrading at higher than 1% per year, excluding the safety failures, are reliability failed modules. All the reliability failed modules qualify for the warranty claims proportional to the rate of degradation. Reliability failures are also called hard failures.
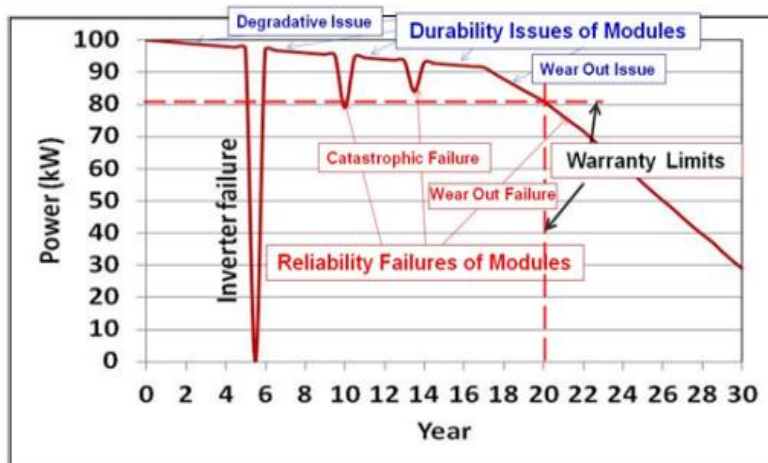
Figure 33. Reliability and Durability Issues of PV Module [14]

2.2.3 Durability Failures

If the performance of a PV module degrades but still meets the warranty requirements, then those losses may be classified as soft losses. All the modules that degrade less than 1% per year, excluding the safety failures, are called durability failed modules. The durability issues are attributed only to the material issues, and the reliability issues are primarily attributed to the design and/or manufacturing issues.

2.2.4 FMEA/FMECA

FMECA is a quantitative approach to determine the dominant failure mode that is observed in the field. FMECA extends FMEA with an addition of a detailed quantitative analysis of criticality of failure modes. FMECA is a method used in a product/system/device to identify the failure modes as they are manufactured using complicated technologies.

43

FMECA is usually conducted in the product design or process development phase, or after a quality function deployment to a product, but conducting it on fielded systems also yields benefits. FMEA/FMECA analysis allows us a good understanding of the behavior of a component of a system, as it determines the effect of each failure mode and its causes, and ranks each failure mode according to criticality, occurrence, and detectability [13].

2.3 METHODOLOGY

2.3.1 System Description

The system was installed in November of 1996 in a cold-dry climate and is currently operational. The 18-year-old system is located on the rooftop of a facility and has a total of 13 arrays, all at latitude tilt (41°). Of the 13 arrays, 12 are actually in use and 1 array has been removed (reason unknown). Within the 12 arrays that are present, 1 combiner box is burnt up, resulting in the entire array producing no power. There are 6 strings in 11 arrays and 2 strings within 1 array, and each string consists of 12 c-Si frameless modules in series. This results in the rated power of each string being 1.44 kW. The operational size of the power plant is 97.92 kW$_{dc}$. The inverter is located inside another building within the facility and is operational.

2.3.2   Site Survey

Visual inspection (VI) was carried out for all 744 modules at this power plant. The VI was performed by using the developed checklist from NREL (National Renewable Energy Laboratory). Defects that were found on every module were noted in the checklist, and a safety map that included all the safety failed modules for the entire site was generated. Every diode was checked in all 744 modules to test for failed diodes that are resulting in open circuited strings. This was conducted using the diode checker. Infrared imaging (IR) was also done using an IR camera for every module at the site. There were no modules that showed any hotspot issues since there was no cell operating at, or above, 20°C of the

average module temperature. For the entire power plant, there were no shading issues that could be found when the SunEye was used.

Both string and module level I-Vs were measured using the Daystar curve tracer and then corrected to STC for this site. The I-Vs for all strings (excluding the 6 strings in the burnt combiner box), for a total of 62 strings, was measured. The total number of modules in this power plant was 744 operational modules. Due to the layout of the power plant, only top row modules were accessible when taking I-V curves, so a total of 46 individual module I-Vs were taken.

As the visual inspection data is obtained, the RPN is calculated to determine the failure modes. The tools and the corresponding accelerated test for the modes are as follows:

Table 7.Various Tools to Identify the Failure Modes

Field failures	Causes/Mechanisms	Characterization Test
Broken Interconnects	Thermal expansion and contraction, repeated mechanical stress	Visual inspection
Broken cells	Mechanical stresses	Electroluminescence (EL)
Corrosion	Moisture induced corrosion of cell metallization	Visual inspection
Delamination	Adhesive bond sensitive to UV or contamination the material	Visual inspection
Encapsulant discoloration	Heat and UV	Visual inspection
Solder bond failures	Stresses induced by thermal cycling or vibration	Visual inspection
Hotspots	Operating current>I_{sc}	Infra-Red scan (IR)
Bypass diode failures		OC diode inspections with handheld device
Backsheet	Visual inspection	

2.3.3 Determination of Severity

Severity depends on two factors – Degradation rate (R_d) and how the failure modes affect the appearance (cosmetic) and performance of the modules, and also safety concerns involved with the failure modes. A rank of 1-7 depends on performance factor and a rank of 8-10 depends on safety factor. A rank of 8-10 forms the highest severity part as they are involved with safety problems created by the failure modes.

The degradation rate is calculated using the formula below:

$$\text{Degradation rate } (R_d) = (P_{max} \text{ drop} * 100)/(\text{Rated } P_{max} * \text{age of operation})$$

The below table gives the Severity ranking corresponding to the degradation rate (R_d).

Table 8. Severity (S) and Detection (D) Ranking Table

Ranking	Detection Criteria	Severity Criteria
1	Monitoring System itself will detect the failure mode with warning	No effect, Rd < 0.3%
2	Very high chance of detection through visual inspection	Insignificant, Rd approx. to 0.3%
3	High chance of detection through visual inspection	Minor Cosmetic defect, Rd < 0.5%
4	Very high chance of detection using a sophisticated tool	Cosmetic defect with Rd < 0.6%
5	Good chance of detection using a sophisticated tool	Reduced performance, Rd < 0.8%
6	Very high chance of detection using multiple sophisticated tool	Performance loss approx. to typical warranty limit, Rd approx. to 1%
7	High chance of detection using multiple sophisticated tool	Significant degradation, Rd approx. to 1.5%
8	Very low chance of detection using multiple sophisticated tool	Remote safety concerns, Rd > 1%
9	Remote chance of detection	Remote safety concerns, Rd > 2%
10	Detection impossible in the field	Safety hazard, Catastrophic

2.3.4 Determination of Detection

The detection ranking is based on how simple/complex it is to determine the field failures.

A rank of 1 is given if the failure mode is determined just by looking at the monitoring

system. If the visual inspection technique is sufficient to determine the failure mode then a

ranking of 2-3 is given. A ranking above 3 is given depending on the tools (ex: IR,

diode/line checker, IV tracer) used, and when the failure is impossible to determine in the field, rank 10 is assumed.

Table 9. Detection (D) Ranking Table

Ranking	Criteria: Likelihood	Detection
1	Monitoring System itself will detect the failure mode with warning 100%	Almost certain
2	Very high probability (most likely) of detection through visual inspection	Very high
3	50/50 probability (less likely) of detection through visual inspection	High
4	Very high probability (most likely) of detection using conventional handheld tool e.g. IR, Megger	Moderately high
5	50/50 probability (less likely) of detection using conventional handheld tool e.g. IR, Megger	Moderate
6	Very high probability (most likely) of detection using non-conventional handheld tool e.g. diode/line checker	Low
7	50/50 probability (less likely) of detection using non-conventional handheld tool e.g. diode/line checker	Very low
8	Very high probability (most likely) of detection using performance measurement equipment e.g. IV tracer	Extremely Low
9	50/50 probability (less likely) of detection using performance measurement equipment e.g. IV tracer	Remote
10	Detection impossible in the field	Absolutely uncertain

2.3.5 Determination of Occurrence

Occurrence denotes the probability of occurrence of a failure mode for a predetermined or stated time period. CNF (Cumulative Number of module Failures per thousand per year) is to be computed.

It is given by:

$$\text{CNF}/1000 = \Sigma \text{system (\% defects)} * 10 \, / \, \Sigma \text{system (operating time)}$$

where,

% of defects = (number of particular defect/ total number of modules)*100

Operating time = duration for which modules are employed

Table 10. Occurrence (O) Ranking Table

Failure Mode Occurrence	Frequency	Ranking O
Remote: Failure is unlikely	<= 0.01 module per thousand per year	1
Low: Relatively few failures	0.1 module per thousand per year	2
	0.5 module per thousand per year	3
Moderate: Occasional failures	1 module per thousand per year	4
	2 module per thousand per year	5
	5 module per thousand per year	6
High: Repeated failures	10 module per thousand per year	7
	20 module per thousand per year	8
Very high: Failure is almost inevitable	50 module per thousand per year	9
	>= 100 module per thousand per year	10

2.4 RESULTS AND DISCUSSIONS

2.4.1 Degradation Analysis of Model-J (String and Module-level)

The histogram shown in Figure 32. provides the mean and median string-level degradation rate of power for Model-J. The histogram fits a near-normal distribution. The average degradation for string level power at this site is found to be 0.73%/year. Out of all 62 strings, 57 strings (92%) are meeting the maximum degradation rate of 1.0%/year typically provided by the module manufactures. The median and average degradations are very close to each other (0.73%/year vs. 0.69%/year), indicating a tight quality management system during production. However, there is an outlier for one string due to the presence of a delaminated backsheet module in the string leading to severe encapsulant delamination causing I_{sc} loss along with voltage loss due to bypass triggering.
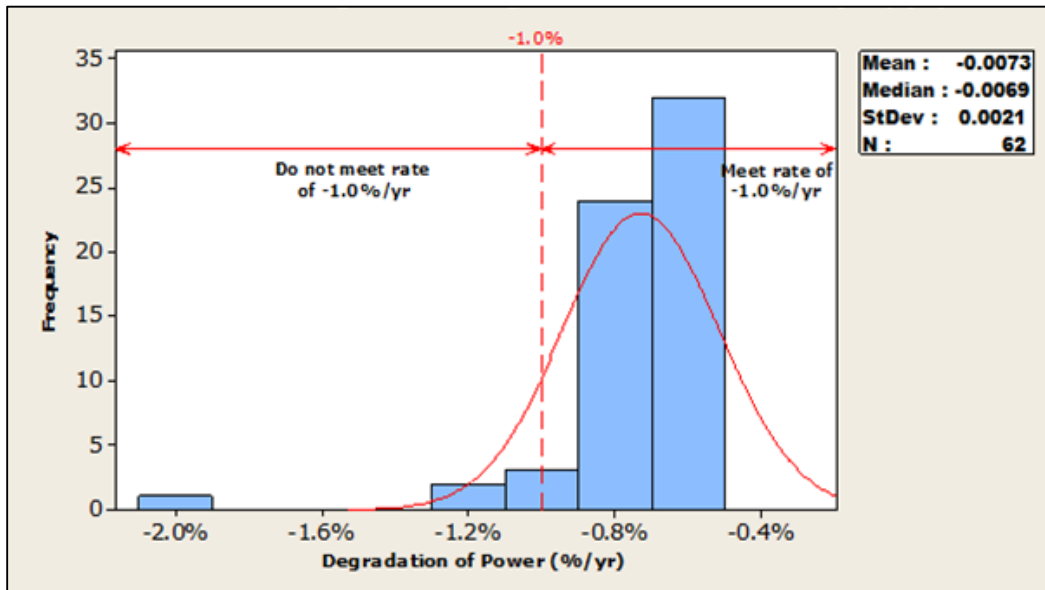
Figure 34. Model-J String-level Degradation of Power

From 46 module I-V curves, the average degradation rate of power is found to be 0.55%/year. Out of 46 modules, 40 modules (86.3%) are meeting the less than 1.0% degradation rate limit typically provided by module manufactures, as shown in Figure 33. The string degradation rate seems to be slightly higher than the module degradation rate due to module mismatch that occurs during string level analysis.
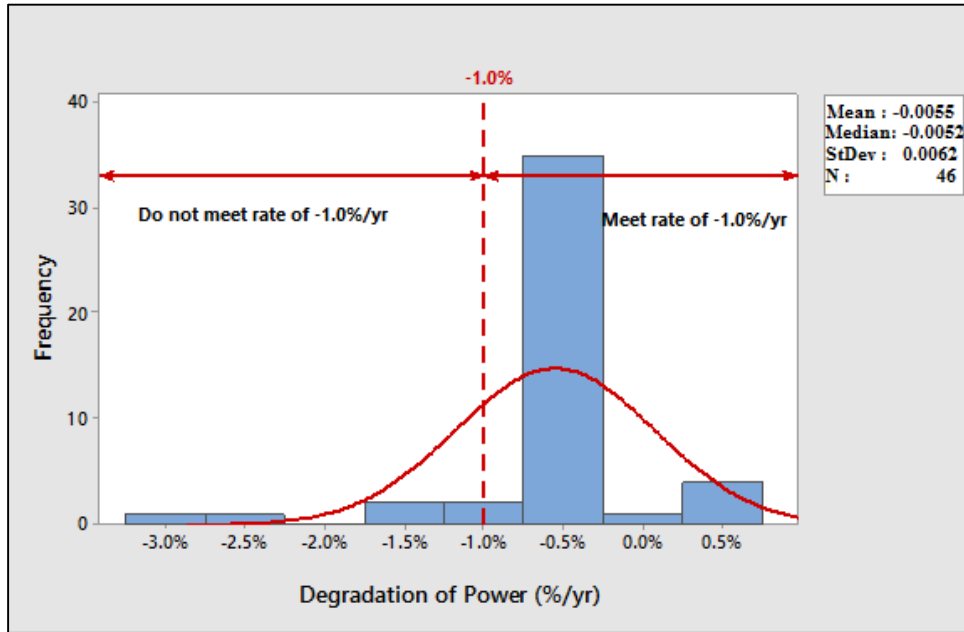
Figure 35. Model-J Module-level Degradation of Power

2.4.2   Layout of Degradation and Safety Failures

The defects that are present in 744 modules are provided in the graph below. Of all, backsheet bubbles, overcell encapsulant delamination and near edge encapsulant delamination are prominent in almost all the modules. Bypass diode failure, broken module and broken cell interconnect (photographs of a few defects shown in Figure 41) are determined to be the safety issues, wherein, the rest of the defects are considered to contribute to the increase in degradation rate.
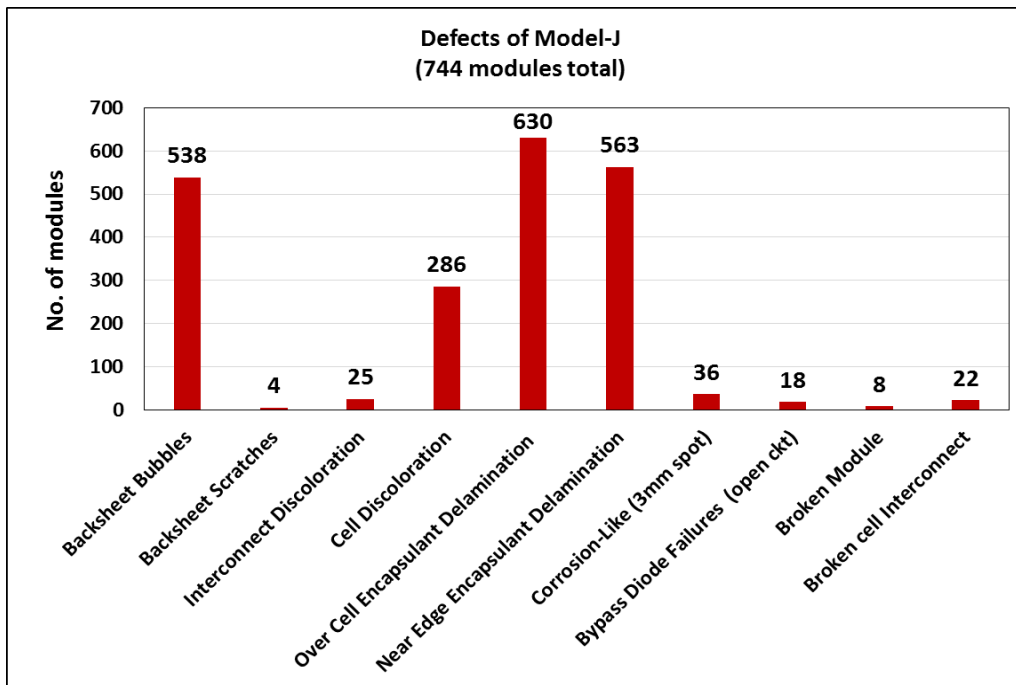
Figure 36. Defects Identified in Model-J

The safety map below shows the safety failures that are found in the power plant, 45 in total. The majority of the issues are found to be due to broken cell interconnects (22 modules) and 18 modules had failed diodes. The 8 broken modules are found to pose a safety hazard due to electrical hazard and mechanical hazard. Broken cell interconnects are a safety hazard due to the possibility for arcing to occur. Failed diodes have the possibility to cause backsheet burning.
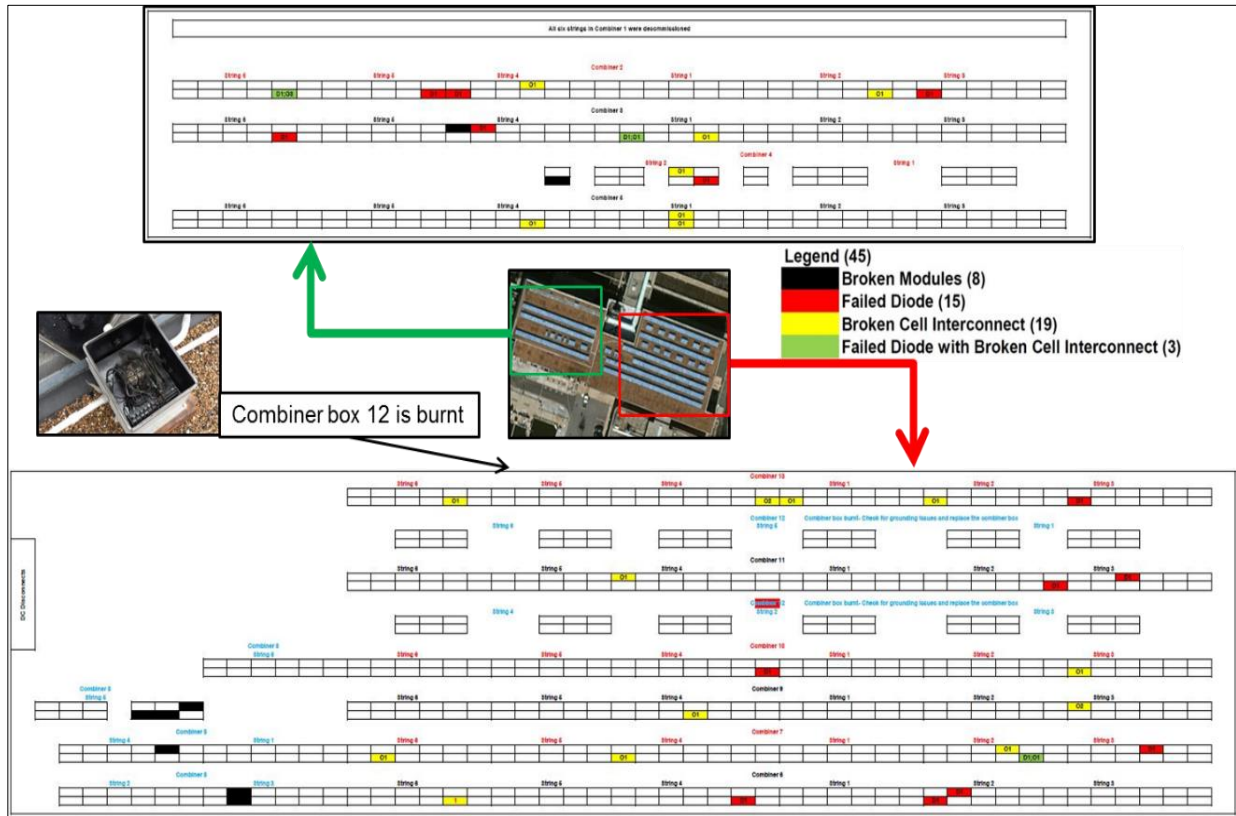
Figure 37. Safety Map for Model-J

When extrapolating the measured module degradation and including the safety failures, 86.3% of the modules are safe and are meeting the manufacturer's warranty, with only 5.5% of modules being safety failures and another 8.7% exceeding the manufacturer's typical warranty of 1%/year degradation rate as shown in Figure 38.
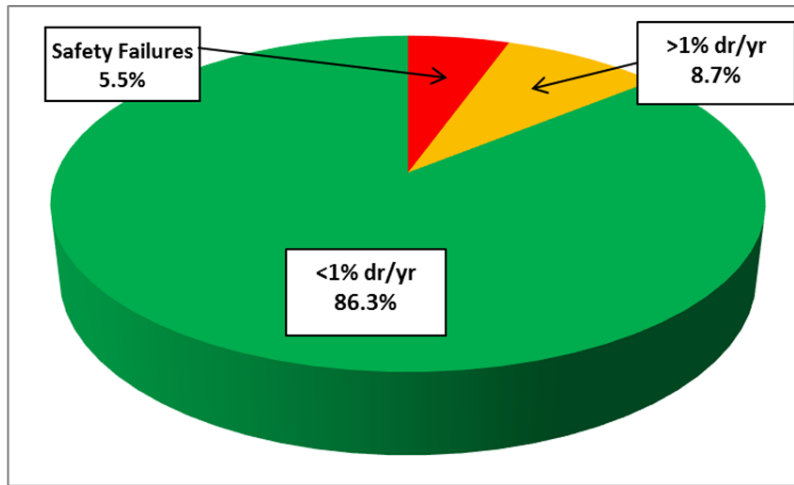
Figure 38. Safety Failures, Reliability Failures and Durability Loss for Entire Power Plant
(Model-J)

2.4.3 String-level RPN Calculation for Model-J

Of all 68 strings, visual inspection and I-V's are taken on 62 strings (excluding the 6 strings in the burnt combiner box), and all the strings present in the plant are evaluated for I-V and VI measurements with Confidence Level (CL) 100% and Confidence Interval (CI) 0%.

The sum of each defect that is present in the above stated 62 strings are considered to be the count. From the count, frequency of occurrence of failure mode is computed using the formula discussed in the previous section. A maximum value of 9 is given to four defects as almost all modules along the string had these defects.

From the degradation data (R_d), severity is calculated. A severity of 10 is given for both broken module and bypass diode failure as a broken module possesses an electrical hazard.

Failed diodes may lead to backsheet burning, so it is considered as a safety issue and a maximum ranking for severity is given.

Depending on how the defects were detected, ranking is given accordingly. As most of the failure modes are detected visually, a ranking of 2 is given. Bypass diode failure alone is determined using diode/line checker and a conventional handheld tool is used, and a ranking of 4 is given.

Table 11. String-level Severity and Occurrence Table for Model-J

Defects	Frequency (%)	Degradation rate (%/Y)	Severity, S	Occurence, O
Backsheet Bubbles	72.31	0.61	5	9
Backsheet Scratches	0.54	0.20	1	3
Interconnect Discoloration	3.36	0.30	2	5
Cell Discoloration	38.44	0.41	3	9
Over Cell Encapsulant Delamination	84.68	0.73	5	9
Near Edge Encapsulant Delamination	75.67	0.59	4	9
Corrosion-Like (3mm spot)	4.84	0.13	1	6
Bypass Diode Failures (open ckt)	2.42	0.54	10	5
Broken Module	1.08	0.32	10	4
Broken cell Interconnect	2.96	0.67	8	5

Figure 40 indicates that RPN is calculated in 3 ways:

1.   Global RPN – gives entire plant RPN (includes both degradation and safety issues)

2.   Degradation RPN – considers defects that contribute only to degradation issues (safety issues are neglected during this RPN calculation)

3.   Safety RPN - considers defects that possess only safety issues (degradation issues are neglected during the safety RPN calculation)

The global string-level RPN for this site is found to be 704 where the degradation RPN contributes to 344 and the safety RPN contributes to 360. Broken glass, broken cell interconnect and bypass diode failures belonging to safety should be immediately considered, and the modules should be replaced depending on the safety threat they possess.
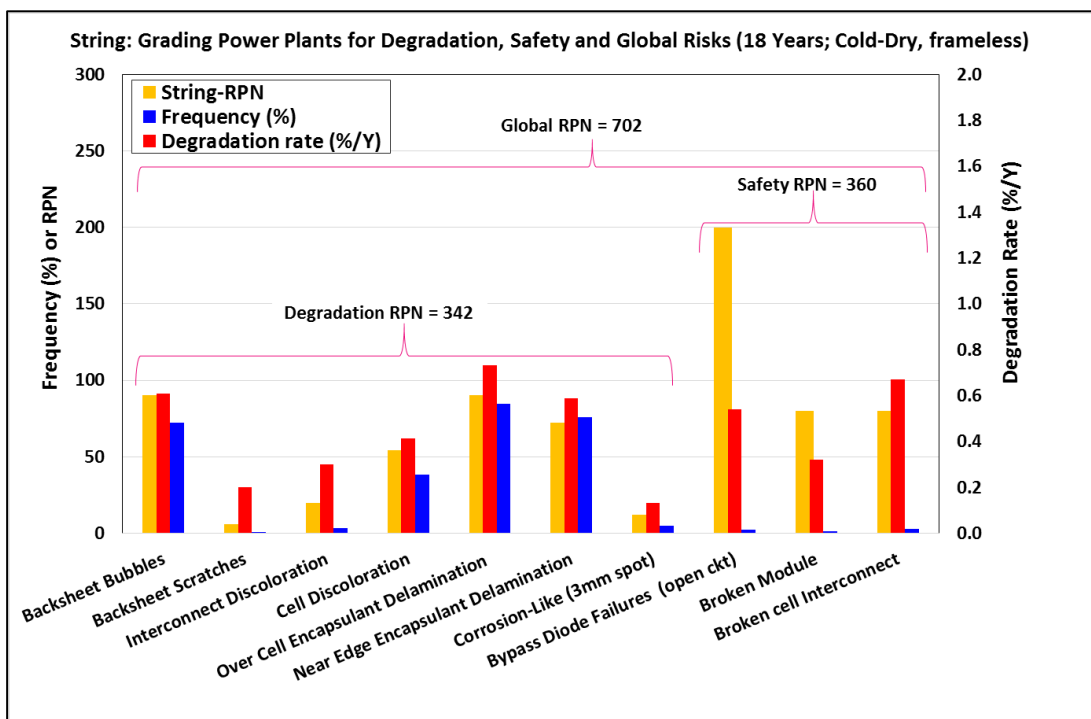
Figure 39. Global, Degradation and Safety RPN Chart for String-level Analysis

2.4.4 Module-level RPN Calculation for Model-J

Due to plant layout and time constraint, only top modules in the strings were accessible and individual I-V's were taken only for 46 modules. Modules that had both I-V and VI data is considered for the module-level RPN analysis. The count and detection ranking is

the same as string-level RPN, but severity ranking that is based on the degradation rate is going to vary.

Few defects (backsheet scratches, corrosion-like, broken module) that are not observed in the calculation of module-level RPN are observed in the string-level calculation. The defects involved in the calculation of module-level RPN are as follows:

Table 12. Module-level Defects for Model-J

Defects	Frequency (%)	Degradation Rate (%/Yr)	Severity, S	Occurrence, O	Detection, D	Module-RPN
Backsheet Bubbles	72.31	0.21	1	9	2	16
Interconnect Discoloration	3.36	0.11	1	5	2	12
Cell Discoloration	38.44	0.22	1	9	2	16
Over cell Encapsulant Delamination	84.68	0.64	5	9	2	90
Near Edge Encapsulant Delamination	75.67	0.31	3	9	2	54
Bypass diode Failures (Open Ckt)	2.42	0.10	10	5	4	200
Broken cell Interconnect	2.96	0.30	8	5	2	80

Module-level RPN is also calculated in a similar manner as string-level RPN. Figure 44 includes only the defects that are present in 46 modules. Figure 42 includes all defects that are present in the strings, but severity of 0 is given if that particular defect is not identified during the module-level calculation.

Figure 40. Global, Degradation and Safety RPN for Module-level
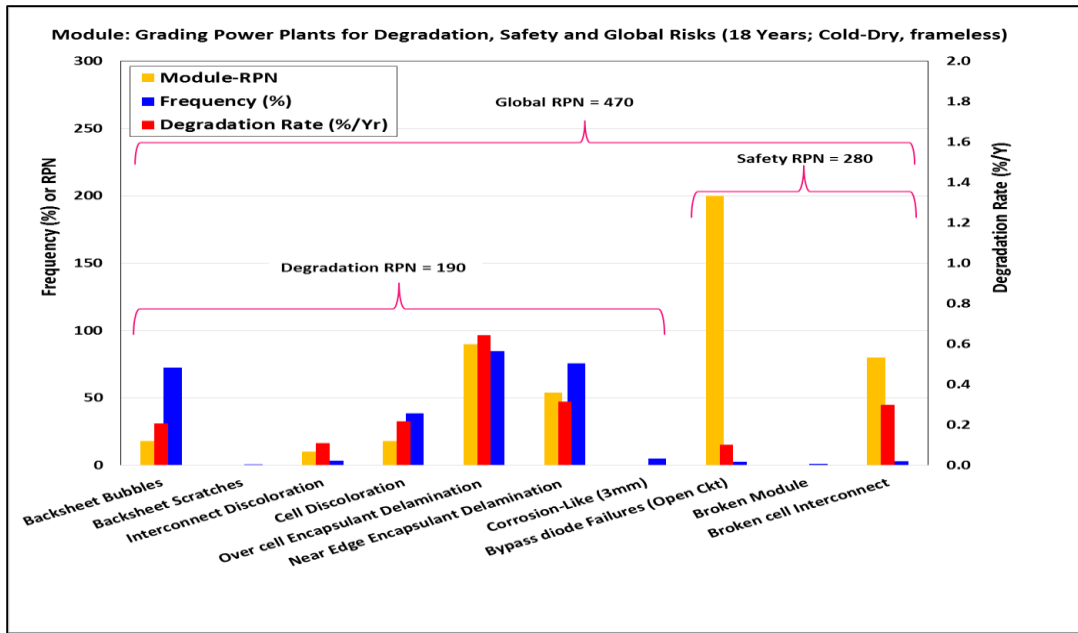
Figure 41. Global, Degradation and Safety RPN for Module-level (all defects included)
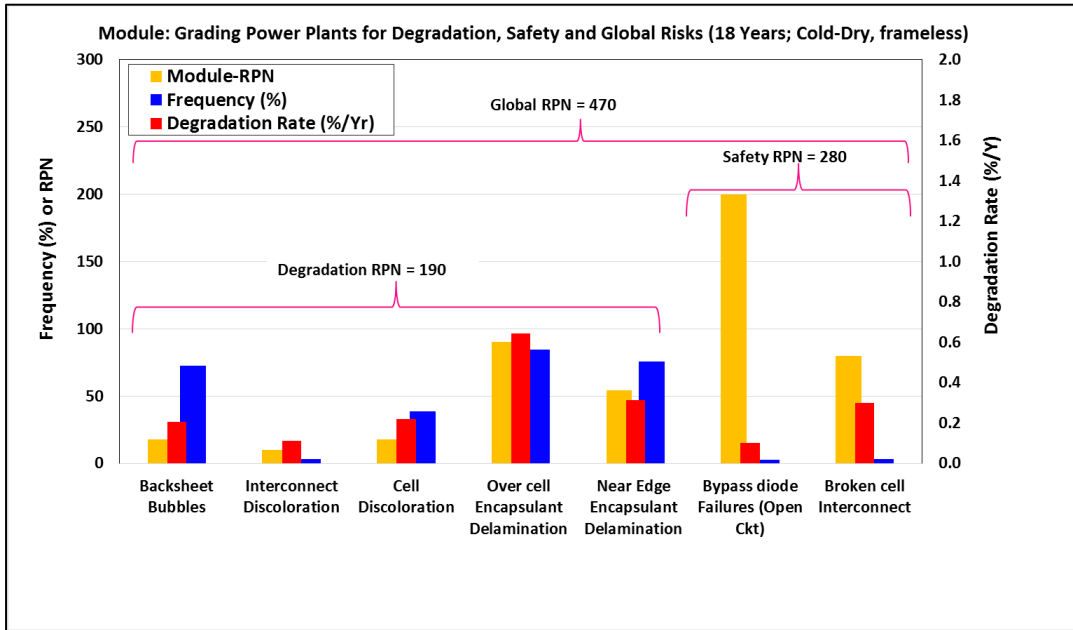
The global string-level RPN for this site is calculated to be 704 and global module-level

RPN is calculated to be 470. Statistically, both string and module-level global RPN should

nearly match, but for this site it does not seem to be true. Only 46 modules were considered for module-level global RPN, but to have a CL (confidence level) of 95% and CI (confidence interval) of 5%, 254 modules should have been considered. Insufficient data for the calculation of module-level global RPN could be one of the reasons for this discrepancy.

2.4.5 Comparison Plots between Model-J and Model-JVA

As indicated in the abstract, the statistical risk analysis of two power plants was jointly performed by two Masters students. Both power plants are located at the same cold-dry climate, but one power plant carries framed modules and the other carries frameless modules as shown in Figure 41. This thesis presented the results on the framed modules. Comparing these two sites would help understand the failure modes and mechanisms for this climatic zone as both the plants had modules from the same manufacturer.

Table 13. Comparison between Model-J and Model-JVA

Variables	Model-J	Model-JVA
Module construction	Frameless	Framed
Place	State of New York (close to water body)	State of New York (higher temperature influence compared to Model-J)
Tilt angle	41º	41º
Age	18 years	19 years
System state	Functional	Not functional

Dominant Failure Mode (degradation)	Over cell Encapsulant Delamination	Interconnect Discoloration and Encapsulant Browning
Degradation Rate (String level)	0.73%/year	0.6 %/year

Model-J, 18-year-old plant had a string-level degradation of 0.73%/year, whereas model-JVA, 19-year-old plant, had a string-level degradation of 0.6%/year. From Figures 45 and 46, it is inferred that the dominant failure mode for model-J is encapsulant delamination; browning and interconnect discoloration for model-JVA. These failure modes are mainly due to moisture ingress. For model-J, intrusion of moisture resulted in backsheet bubbles that further lead to encapsulant delamination. Encapsulant delamination resulted in optical decoupling that not only had an effect on I_{sc} drop, but also on V_{oc} drop, resulting in triggering of bypass diodes. Due to high V_{oc} drop, the number of diodes failed in model-J is higher compared to model-JVA (Table 15). This comparative study between framed and frameless modules of the same model in cold-dry climate clearly indicates that the frameless modules are highly susceptible to backsheet delamination leading to severe encapsulant delamination. The severe encapsulant delamination leads to high I_{sc} drop, high V_{oc} drop (due to bypass triggering) and high bypass diode failures, as they conduct electricity during daytime every day for several years before they permanently fail under open circuit conditions.

Interconnect discoloration is scarcely found in model-J because a frameless module (Figure 43) does not have a leakage current path as the mounting rail is on the backskin of PV modules. In the case of a framed module, current leakage occurs between cell and frame through electrolytic corrosion, resulting in interconnect discoloration. These modules should have higher series resistance problems leading to local I^2R heating, which, in turn, leads to encapsulant browning (Figure 44).
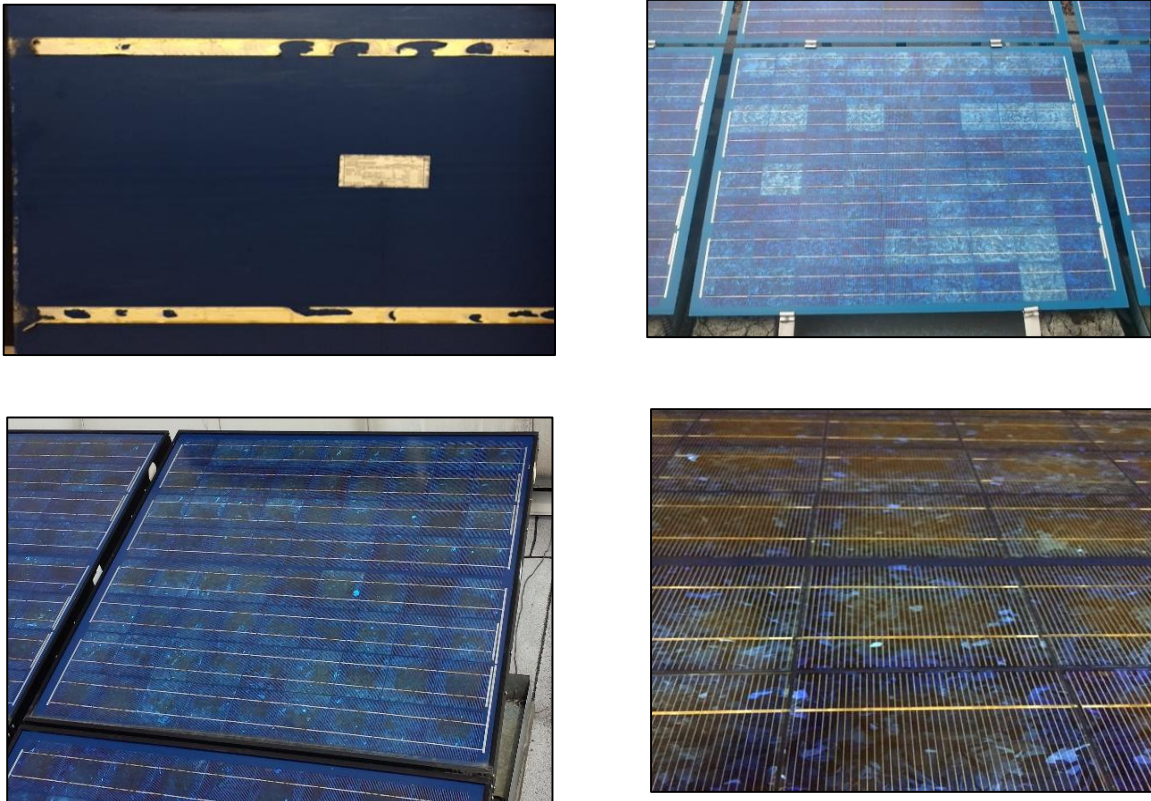
Figure 42. (clock-wise) a) Backrail Mounting using Adhesive of Frameless Module Model-J b) Framed Module at Model-JVA; c) Encapsulant Browing and Interconnect Discoloration in Model-JVA; d) Encapsulant Delamination in Model-J
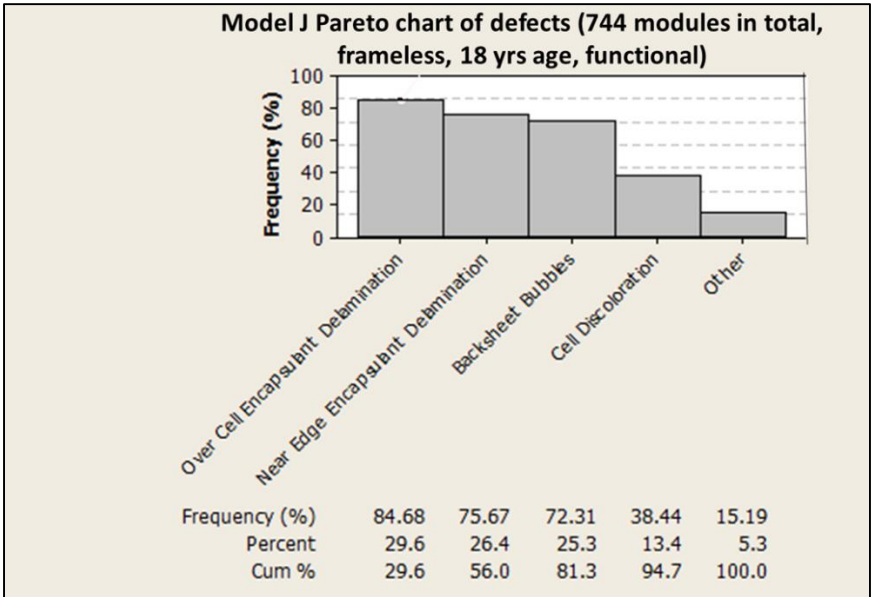
Figure 43. Pareto Chart for Model-J

Frequency (%)	84.68	75.67	72.31	38.44	15.19
Percent	29.6	26.4	25.3	13.4	5.3
Cum %	29.6	56.0	81.3	94.7	100.0

Frequency (%)	50.00	45.69	33.05	24.71	8.62	23.28
Percent	27.0	24.7	17.8	13.3	4.7	12.6
Cum %	27.0	51.6	69.5	82.8	87.4	100.0
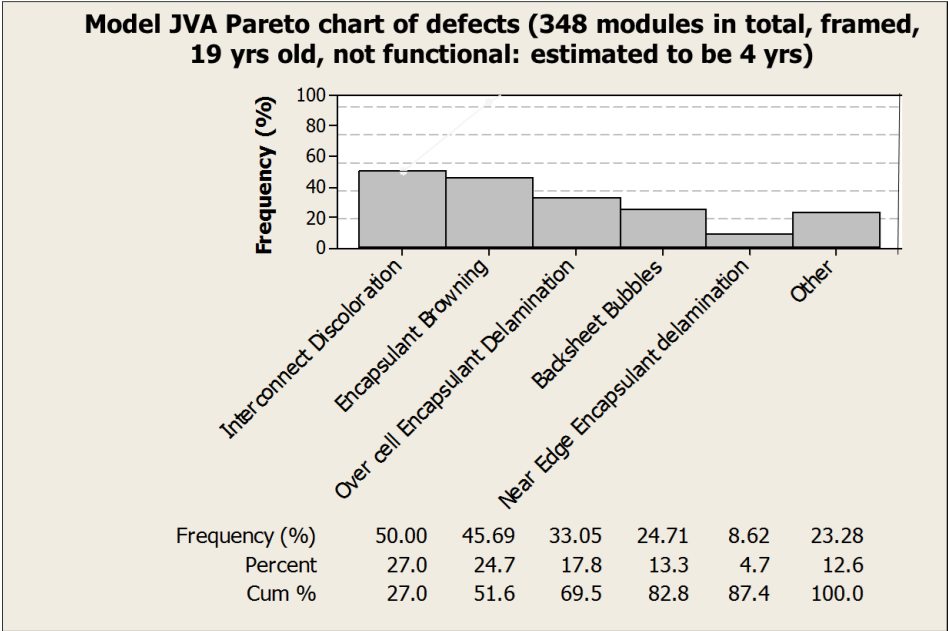
Figure 44. Pareto Chart for Model-JVA

2.5 CONCLUSION

- Model-J is an 18-year-old power plant in a cold-dry climatic condition, having string-level degradation of 0.73%/year and module-level degradation of 0.55%/year.

- The global RPN for the power plant is divided into safety and degradation RPN. For model-J, string-level global RPN was determined to be 704 and module-level global RPN was calculated to be 470.

- For cold-dry climatic conditions, the degradation rate is about 0.6% per year (framed) to 0.73% per year (frameless).

- Encapsulant delamination was the dominant failure/degradation mode for frameless modules, while interconnect discoloration was the dominant degradation mode for framed modules. However, both these modes are the result of extent of moisture ingress.

REFERENCES

[1]   Travis Sarver, AliAl-Qaraghuli, Lawrence L. Kazmerski, "comprehensive review of the impact of dust on the use of solar energy: History, investigations, results, literature, and mitigation approaches", Renewable and Sustainable Energy Reviews, March 15, 2013.

[2]   J. Zorrilla-Casanova, M. Piliougine, J. Carretero, P. Bernaola, P. Carpena, L. Mora-López, M. Sidrach-de-Cardona, "Analysis of dust losses in photovoltaic modules", World Renewable energy Congress, Sweden, 2011.

[3]   P. D. Burton and B. H. King, "Application and Characterization of an Artificial Grime for Photovoltaic Soiling Studies," IEEE Journal of Photovoltaics, vol.4, No.1, pp. 299-303, Jan 2011.

[4]   B. Sopori, Y. Zhang, R. Faison, and J. Madjdpour, "Principles and Applications of Reflectometery in PV Manufacturing", National Renewable Energy Laboratory, October 2001.

[5]   D. Summers, M. Lewis, B. Ostendorf, D. Chittleborough, "Visible near-infrared reflectance spectroscopy as a predictive indicator of soil properties", May 5, 2009.

[6]   http://manuals.harborfreight.com/manuals/94000-94999/94572.pdf

[7]   http://www.asdi.com/products/fieldspec-spectroradiometers/fieldspec-4-hi-res

[8]   http://support.asdi.com/Document/Viewer.aspx?id=140

[9]   B. Knisley, "Angle of Incidence and Non-Intrusive Cell Quantum Efficiency Measurements of Commercial Photovoltaic Modules," MS thesis, Arizona State University, December 2013.

[10]   http://www.pvmeasurements.com/Quantum-Efficiency-Measurements/qex12m-solar-module-quantum-efficiency-measurement-system.html

[11]   Sravanthi Boppana, Vidyashree Rajashekar, Govindasamy Tamizhmani, "Working towards the Development of a Standardized Artificial Soiling Method" Accepted, IEEE PVSC, New Orleans, 2015.

[12]   S.A Bowers, R J Hanks, "Reflection of radiant energy from soils," Soil Science, vol. 100, 130-138, 1965.

[13]   Sanjay Mohan Shrestha, Jaya Krishna Mallineni, Karan Rao Yedidi, Brett Knisely, Sai Tatapudi, Joseph Kuitche, and GovindaSamy TamizhMani, "Determination of Dominant Failure Modes Using FMECA on the Field Deployed c-Si Modules Under Hot-Dry Desert Climate", IEEE Journal of Photovoltaics, vol. 5, no. 1, January 2015.

[14]   G. TamizhMani and J. Kuitche, "Accelerated Lifetime Testing of Photovoltaic Modules" A report of Solar America Board for Codes and Standards (solarabcs.org), 2013.

APPENDIX A

CHEMICAL COMPOSITION AND PARTICLE SIZE OF ARIZONA ROAD DUST

PTI
POWDER TECHNOLOGY INC.

PRODUCT LIST PP2G4
ISO 12103-1 ARIZONA TEST DUST CONTAMINANTS A2 FINE AND A4 COARSE GRADES

TYPICAL CHEMICAL ANALYSIS

Chemical	% Of Weight	Chemical	% Of Weight
SiO_2	68 - 76	CaO	2.0 - 5.0
Al_2O_3	10 - 15	MgO	1.0 - 2.0
Fe_2O_3	2 - 5	TiO_2	0.5 - 1.0
Na_2O	2 - 4	K_2O	2.0 - 5.0

*Loss on Ignition 2 – 5%

ISO TEST DUST PARTICLE SIZE DISTRIBUTIONS BY VOLUME %

SIZE (µm)	ISO 12103-1, A2 Fine (% less than)	ISO 12103-1, A4 Coarse (% less than)
1	2.5 – 3.5	0.6 – 1.0
2	10.5 – 12.5	2.2 – 3.7
3	18.5 – 22.0	4.2 – 6.0
4	25.5 – 29.5	6.2 – 8.2
5	31.0 – 36.0	8.0 – 10.5
7	41.0 – 46.0	12.0 – 14.5
10	50.0 – 54.0	17.0 – 22.0
20	70.0 – 74.0	32.0 – 36.0
40	88.0 – 91.0	57.0 – 61.0
80	99.5 – 100	87.5 – 89.5
120	100	97.0 – 98.0
180	-	99.5 – 100
200	-	100

APPENDIX B

STANDARD OPERATING PROCEDURE FOR REFLECTANCE

Applications

This procedure shall be used in all indoor and outdoor Reflectance and Transmittance measurements using HandHeld FieldSpec 4 Wide-Res spectroradiometer.

Procedure - Reflectance

1. In the rear portion of the spectroradiometer unit, connect the power supply to the input 12 VDC port. Also, connect the Ethernet cable to the appropriate port with the other end connected to the laptop. (Ensure that the laptop is always switched on after the spectroradiometer.)

Figure B1. Power supply to port connection

2. Connect the accessory power port to the contact probe as shown below.

3. To connect the fiber optic, first remove the screws in such a manner that the grey color screw is placed in the same place. Then take the fiber optic and insert it in the screw that has been removed. Gently push the fiber optic in the place were the screws were already present and tighten it. **(Handle the fiber optic with utmost care as it is sensitive and tends to break.)**

71

Figure B2. Handling of fiber optic

Figure B3. Step-by-step process of inserting optic fiber to the contact probe

4. Hit the 'ON' button, which is on the rear side of the spectroradiometer unit, and then click the 'ON' button that is present on the contact probe so that the instrument starts warming up. For reflectance measurements, the light source should be

switched on for a minimum of 15 minutes, whereas for radiometric measurements, the time is extended to an hour.

Figure B4. Switching and warming up of the instrument

5. Even for outdoor measurements, initially use the power supply as the source and then once the instrument is warmed up, the battery can be used. The battery is charged separately by connecting one end of the power cord to the battery and the other end to the supply. As in step 1, instead of connecting the power supply to 12VDC, connect the battery in its place.

Figure B5. Charging of battery

6. Once the instrument is warmed up, take a small square-shaped, black colored cardboard/sheet and make a circle in the center the same as the size of the lens. Insert it to avoid the entry of the stray light and then clean the lens using lens wipes (Isopropyl alcohol and a soft cloth). Switch on the laptop.

Figure B6. Cleaning of lens

OPTIMIZATION AND WHITE REFERENCE:

Before taking any reading, first you need to optimize the instrument to the current atmospheric conditions. (If you are doing an outdoor experiment, take the instrument outdoors and optimize it, as the indoor and outdoor atmospheric conditions differ).

Optimize the instrument whenever the atmospheric conditions differ or whenever a beep sound comes from the instrument indicating that the instrument is saturating.

1. Cover the lens of the contact probe using white reference (WR). Never touch the central white portion of the WR as it is already calibrated. Then hit the RS^3 software in the desktop. (There are two RS^3 software in the desktop; click high contrast for outdoor measurements.)

Figure B7. White reference measurement

2. A dialog box appears. Using the drop down menu, change the settings to bare fiber and raw DN mode. Then hit the 'OPT' (Optimize) to go ahead with the optimization.
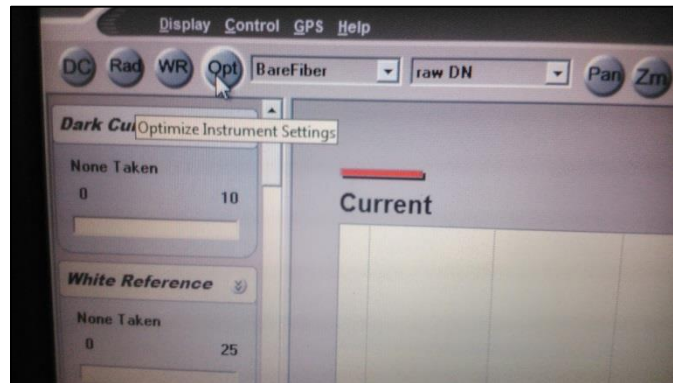
Figure B8. Dialog box to change settings

3. Once optimization is done, then click the 'WR' (White Reference) which is right next to the 'OPT'. After collecting the WR, you get an image as below. A straight line appears at reflectance 1, indicating that the spectroradiometer unit has reflected all the light that it has encountered.

DATA COLLECTION:

Then the WR cap is removed and the contact probe is placed perpendicular to the sample for which the reflectance measurements are to be made. For saving the measurements, go to Control -> Spectrum save -> Dialog box appears -> Give the file name and check for the dates -> Hit Begin Save. The measurements start saving and for each and every spot on the sample you will have 10 readings.

Figure B9. Reflectance measurement on module

CONVERSION OF ASD TO TXT FILES:

Once all the measurements are done, the reflectance values are saved as ASD files and the next step is to convert them to TXT files. Go to ViewSpec Pro -> File -> Open (open the files you want to convert) -> Process -> ASCII Export -> In the dialog box, just change the Data for .asd files only to Reflectance (don't change any) -> OK.

The Output path where the processed data gets stored is indicated at the bottom of this software.
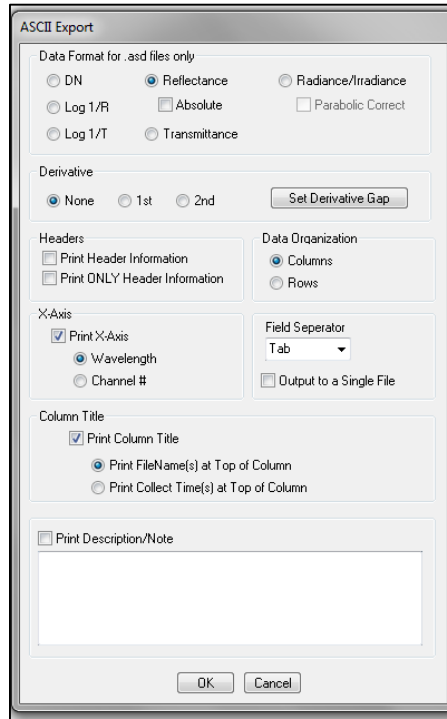
Figure B10. Exporting of .asd files

NOTE: For any further information about the Spectroradiometer, click on the below link

to access the user manual;

http://support.asdi.com/Document/Viewer.aspx?id=140